CrossMark

ORIGINAL PAPER

Inclined transpression in the Neka Valley, eastern Alborz, Iran

Seyed Tohid Nabavi[1] · Manuel Díaz-Azpiroz[2] · Christopher J. Talbot[3,4]

Abstract Three major nappes in the Neka Valley in the eastern Alborz Mountains of Iran allow the Cimmerian to present convergence following the oblique collision between Iran and the southern margin of Eurasia. This work reports the identification of an inclined transpression zone recognized by field investigations and strain analyses of the geometries of formations and detailed mesoscopic structural analyses of multiple faults, folds and a cleavage. The main structures encountered include refolded recumbent asymmetric fold nappes, highly curved fold hinges, in a transpression zone that dips 37° to the NW between boundaries thrusts striking from N050° to N060°. The β angle (the angle between the zone boundary and direction of horizontal far-field shortening) is about 80°. The northwest and south-east boundaries of this zone coincide with the Haji-abad thrust and the Shah-Kuh thrust, respectively. Fold axes generally trend NE–SW and step to both right and left as a result of strike–slip components of fault displacements. Strain analyses using Fry's method on macroscopic ooids and fusulina deformed into oblate ellipsoids indicate that the natural strain varies between 2.1 and 3.14. The estimated angle between the maximum instantaneous strain axis (ISA_{max}) and the transpression zone boundary (θ') is between 6° and 20°. The estimated oblique convergence angle (α), therefore, ranges between 31° and 43°. The average kinematic vorticity number (W_k) is 0.6, in a zone of sinistral pure shear-dominated inclined triclinic transpression. These results support the applicability of kinematic models of triclinic transpression to natural brittle–ductile shear zones.

Keywords Inclined transpression · Strain analysis · Strain partitioning · Neka Valley · Eastern Alborz

Introduction

From a kinematic point of view, transpression has been defined as a strike–slip deformation that deviates from simple shear (Mukherjee and Koyi 2009; Mukherjee 2011a, b, 2012a, b, 2014a, b, c; Mukherjee and Mulchrone 2012; Mulchrone and Mukherjee 2015) because of shortening orthogonal to the deformation zone and/or extension along it (Sanderson and Marchini 1984; Fossen and Tikoff 1993; Tikoff and Fossen 1993; Dewey et al. 1998; Schulmann et al. 2003; Mukherjee 2007). Most geological transpression is driven by the oblique convergence of lithospheric plates. Transpression occurs on a wide variety of scales from lithospheric plate downwards in any strike–slip zone that is not perfectly planar (Harland 1971; Dewey 1988; Mukherjee and Biswas 2014, 2015). Transpression zones are often active after the orogenic thickening stage and can play an important role in the exhumation of high-grade metamorphic rocks (Oldow et al. 1990; McCaffrey 1992; Woodcock and Schubert 1994; Dewey et al. 1998; Carosi and Palmeri 2002; Carosi et al. 2004, 2005; Jones et al. 2004, 2005; Zibra et al. 2014; Dasgupta et al. 2015). Systems of oblique

✉ Seyed Tohid Nabavi
  Tohidnabavi@gmail.com; T_nabavi@sbu.ac.ir

1 Department of Geology, Faculty of Earth Sciences, Shahid Beheshti University, Tehran, Iran

2 Departamento de Sistemas Físicos, Químicos y Naturales, Universidad Pablo de Olavide, Carretera de Utrera km 1, 41013 Seville, Spain

3 Hans Ramberg Tectonic Laboratory, Department of Earth Sciences, Uppsala University, Villavägen 16, 75236 Uppsala, Sweden

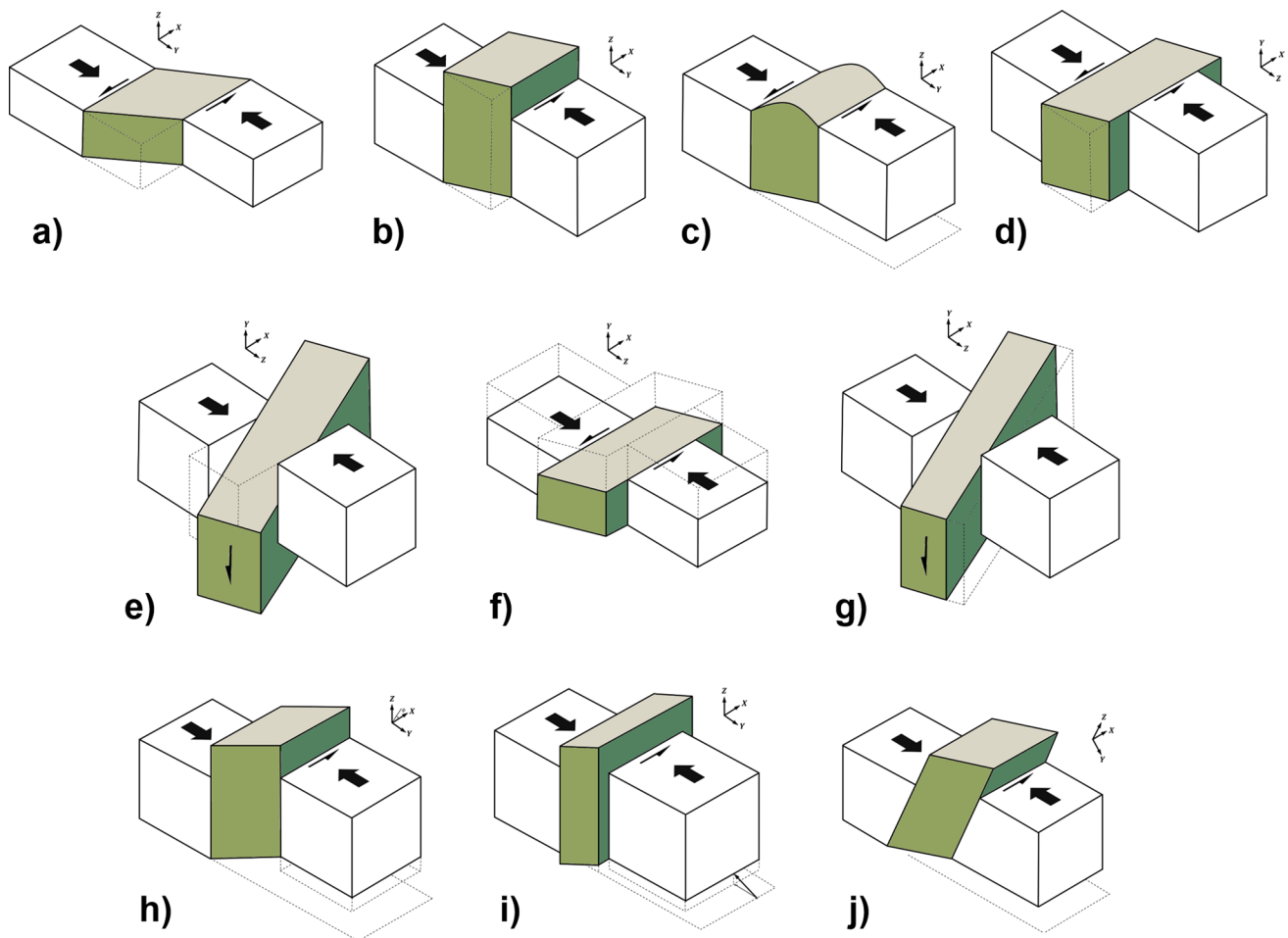4 Present Address: 14 Dinglederry, Olney MK46 5ES, UK

Fig. 1 Models of transpression discussed in text. Reference frame: *X* axis is parallel to the strike of the shear zone boundary, *Y* axis is normal to the boundary, and *Z* axis is parallel to the dip of the zone. *Full arrows* represent the shortening normal to the deformation zone associated with the pure shear component. The *half arrows* represent the simple shear component. **a** Strain geometry of monoclinic thinning zone comparable with Ramsay and Graham's (1970) simple shear zone; **b** monoclinic transpression (Sanderson and Marchini 1984; Fossen and Tikoff 1993); **c** model with no-slip boundaries (Robin and Cruden 1994; Dutton 1997); **d** transpression with lateral escape (Dias and Ribeiro 1994; Jones et al. 1997); **e** transpression with lateral escape and an extra shear component, accounting for axial depression (Dias and Ribeiro 1994); **f, g** transpression with lateral escape and volume change (Dias and Ribeiro 1994); **h** triclinic transpression (Lin et al. 1998; Jiang and Williams 1998). ϕ Is the component of the velocity vector parallel to the shear boundary and the strike of the shear zone; **i** triclinic transpression with inclined simple shearing and inclined extrusion direction (Férnandez and Díaz-Azpiroz 2009); **j** inclined transpression (Jones et al. 2004)

convergence are often associated with transpressional and transtensional structures in wide orogenic zones like the still active Zagroz and Alborz Mountain Ranges in Iran (Teyssier et al. 1995; Tikoff and Greene 1997; Díaz-Azpiroz and Fernández 2005; Giorgis et al. 2005; Sullivan and Law 2007; Sarkarinejad and Azizi 2008; Zibra et al. 2014).

The simplest model of transpression (Ramsay and Graham 1970) is likely to be very common in nature and involves homogeneous deformation without any volume change between a free-slip upper horizontal surface and a fixed lower horizontal boundary (Fig. 1a). In this model, the total regional strain partitions into local domains that accommodate different parts of the bulk strain by transpression and transtension

(e.g. Lister and Williams 1983; Jones and Tanner 1995; Curtis 1997, 1998; Carreras et al. 2013; Dasgupta et al. 2015). Transpressional zones in the upper crust exhibit a wide variety of structures that include positive flower structures with ductile folds (Mukherjee 2014d), as well as strike–slip, reverse and normal faults. Strike–slip faults usually sub-parallel the main boundaries while reverse faults and/or folds form orthogonal to the maximum horizontal infinitesimal stretching direction (Tikoff and Paterson 1998; Frehner 2016). Except where they bound pure contraction zones, the flanking strike–slip, reverse faults usually rotate during progressive deformation, whereas normal faults form and remain at high angle to the zone boundaries (e.g. Sanderson and Marchini 1984; Naylor

et al. 1986; Sylvester 1988; Woodcock and Schubert 1994; Tikoff and Peterson 1998; Díaz-Azpiroz and Fernández 2005; Balanyá et al. 2007; Titus et al. 2007; Sanderson 2014; Frehner 2016). Transpressional zones in the middle or lower crustal ductile are characterized by either strike- or dip-parallel or both lineations. In an ideal vertical shear zone subjected to monoclinic transpression, the attitude of the main lineation depends on the angle of convergence and the amount of accumulated deformation (Sanderson and Marchini 1984; Fossen and Tikoff 1993; Simpson and De Paor 1993; Tikoff and Fossen 1993; Type B in Fossen and Tikoff 1998; Passchier 1998; Teyssier and Tikoff 1999; Tikoff and Fossen 1999; Ghosh 2001; Dewey 2002; Schulmann et al. 2003) (Fig. 1b).

Changes in the angle of convergence may induce different ratios of simple shear to pure shear that can be measured using the kinematic vorticity number (W_k). Fossen and Tikoff (1993) differentiate between simple shear-dominated ($1 > W_k > 0.71$) and pure shear-dominated ($W_k < 0.71$) transpression. However, some natural shear zones have oblique lineations that cannot be explained by monoclinic models (e.g. Hudleston et al. 1988; Goodwin and Williams 1996; Lin et al. 1998; Czeck and Hudleston 2003, 2004; Horsman et al. 2008). This and such other features as the coexistence of apparent constrictional and flattening strain ellipsoids in the same zone (Dias and Ribeiro 1994) are better approximated by progressively more realistic triclinic models that have been constructed by adding a succession of new variables to the boundary conditions of the basic model as indicated in Fig. 1. These models allow for factors such as heterogeneous deformation, slip and no-slip boundaries with maximum vertical extension along the central plane (Fig. 1c after Robin and Cruden 1994; Dutton 1997), lateral stretch in the horizontal (Fig. 1d, e after Dias and Ribeiro 1994; Jones et al. 1997; Type E in Fossen and Tikoff 1998; Tikoff and Fossen 1999), volume changes (Fig. 1f, g after Dias and Ribeiro 1994; Fossen and Tikoff 1998; Jiang et al. 1998, 2001; Fernández and Díaz-Azpiroz 2009; Fernández et al. 2013), oblique simple shear (Fig. 1h after Jiang et al. 1998; Jones and Holdsworth 1998; Lin et al. 1998; Iacopini et al. 2007; Fernández and Díaz-Azpiroz 2009), oblique extrusion (Fig. 1i after Fernández and Díaz-Azpiroz 2009) or inclined transpression with two, strike- and dip-parallel, simple shear components (Fig. 1j after Jones et al. 2004).

In order to better understand transpressional kinematics, it is worth trying to assign natural cases to particular or different combination of the whole range of theoretical models. Most natural active and past shear zones appear to involve strike–slip-dominated shear (e.g. San Andreas system, North America Cordillera), obliquely converging collisional orogens (e.g. Himalayas, Kaoko belt in Namibia) or lateral branches of curved orogens (e.g. Betics, Variscan orogen of SW Iberia). By contrast, only some fold-and-thrust belts have been studied from the perspective of oblique convergence (e.g. Mohajjel and Fergusson 2000;

Sarkarinejad and Azizi 2008; Barcos et al. 2015). In particular, nappe complexes emplaced by rear compression have been rarely considered as transpressional zones (e.g. Rodriguez et al. 2005) as we shall do here.

This paper presents new structural data and strain analyses of a nappe complex at the eastern part of the Alborz Mountains Range (northern Iran). Other transpressional systems in Iran include the Zagros fold-and-thrust system that is a mainly a dextral transpressional orogen. The Zagros Mountains are related to the Late Cretaceous to Tertiary oblique collision and subsequent convergence between the African-Arabian continent and the Iranian microcontinent (Mohajjel and Fergusson 2000). Local sinistral shears in the SE part of the Zagros fold-and-thrust system have been attributed to inclined transpression acting on a curvilinear boundary (Sarkarinejad and Azizi 2008; Sarkarinejad et al. 2013). Dextral transpression has been identified also as part of the polyphase deformation history of the Sanandaj–Sirjan metamorphic belt in the Zagros fold-and-thrust belt in the High Zagros Mountains (e.g. Mohajjel and Fergusson 2000; Mohajjel et al. 2003; Sarkarinejad 2007; Sarkarinejad et al. 2008, 2010a, b; Axen et al. 2010; Babaahmadi et al. 2012; Moosavi et al. 2014; Shafiei Bafti and Mohajjel 2015). Other cases of N–S to NE–SW dextral transpression in Iran occur along the boundary between the Lut and Tabas blocks in central Iran (Cifelli et al. 2013) and W–E to NW–SE transpression along the western-central Alborz Mountains Range (Axen et al. 2001; Allen et al. 2003; Ritz et al. 2006; Zanchi et al. 2006; Ritz 2009; Landgraf et al. 2009; Ballato et al. 2011, 2013). Nabavi et al. (2014) were the first to collect strain data from the Alborz Mountains and to propose a geometric model.

The present work expands this topic by focusing on detailed mesoscopic field analyses and analyses of finite strains, strain partitioning and patterns of strain variation in some of the brittle–ductile nappes in the external part of the eastern Alborz Mountains Range. We analyse the spatial relationships between faults, folds and cleavage with the aim of recognizing interaction between different structures. Our main objectives are: (1) to measure Flinn's k values describing the shape of strain ellipsoids, (2) to estimate the kinematic vorticity number in order to constrain the components of pure shear and simple shear and the strain partitioning pattern in the Neka Valley, (3) to propose a conceptual model for this zone that contributes to a better understanding of the oblique collision between Eurasia and Arabia in the past and their current convergence; and (4) of oblique fold-and-thrust belts in general.

Geological setting

The Alborz Mountains Range is a Cenozoic fold-and-thrust belt along the northern edge of Iran. It records the Eocene and

late Oligocene collision and subsequent convergence between the Eurasian and Arabian plates. This mountain range forms a composite central portion of the Alpine–Himalayan belt that underwent shortening and uplift during Tertiary or Alpine orogeny (Alavi 1996). The major pre-Cenozoic tectonic event in this region occurred when the Paleo-Tethys Ocean between the Iran and Eurasia plates closed in the Late Triassic (Berberian and King 1981). The belt was affected by polyphase deformation, from Eo-Cimmerian orogeny to late Tertiary–Quaternary intracontinental transpression that is still active as shown by GPS measurements (Jackson et al. 2002; McClusky et al. 2003; Vernant et al. 2004) and by active seismicity (Allen et al. 2003; Zanchi et al. 2006, 2009; Berra et al. 2007). The Alborz Mountains range is approximately 600 km long, 100 km wide and 3–5 km high. It is shaped like an Australian boomerang with two "arms" of the Alborz, trending W–E and, NE–SW along the southern shore of Caspian Sea (Allen et al. 2004; Horton et al. 2008). It has a crustal thickness of only 35–40 km; this is unusually thin for such a wide and high mountain range and suggests that no lithospheric root compensates the Alborz Mountains Range (Dehghani and Makris 1984; Guest et al. 2007). In addition, young intrusive magmatism such as late Miocene (Alam Kuh) and Pliocene (Damavand) occurred in the Alborz Mountains (Fig. 2a) (Allen et al. 2003, 2004).

The study area is located south of Gorgan County, in the eastern part of the Alborz Mountains Range (Fig. 2b) between the Radekan and North Alborz faults. It includes rock units mainly from Devonian to Quaternary in age (Fig. 2c). Devonian rocks of the Khosh Yeilagh Formation (conglomerates, sandstones, limestones) are covered by the Lower Carboniferous Mobarak Formation, with limestones at the base passing to well-bedded dark limestones at the top. The Quezel-Qaleh Formation (limestone, oolitic, sandy limestone) of Middle Carboniferous age passes upward to carbonate and terrigenous facies. The Quezel-Qaleh Formation occurs at the base of the Permian succession. The Permian successions appear at the base the Doroud Formation (red conglomerates, sandstones, silty limestones and limestones with fusulinids) (Zanchi et al. 2009). Bedded to massive limestones of the Ruteh Formation and dolomitic limestones and dolostones of the Elika Formation constitute the upper part of the Permian succession. The Early Jurassic Shemshak Formation includes sandstones, shales, clays and coal, and it is followed by continental, lacustrine and lagoon sequences. The Lower Carboniferous Mobarak Formation is not exposed in the study area, but can be found to the north-west, where the sandy and inoceramous-bearing limestones of the Late Cretaceous Ghalemoran Formation unconformably overlies it (Fig. 3a, b).

The Ghalemoran Formation is only slightly deformed and unconformably covers the strongly deformed Mobarak Formation that lacks significant metamorphism and, beneath that, a folded and unmetamorphosed succession of Palaeozoic to Middle Triassic red nodular limestones. Tight to isoclinal folds with steep axial planes are developed within the well-bedded limestones of the Mobarak Formation (Nabavi 2012). This unconformity is well exposed within the study area (Fig. 3a, b) and formed during the Eo-Cimmerian orogeny, when Iran collided with Eurasia during the Mid-Late Triassic (Berra et al. 2007; Zanchi et al. 2009). A high-angle reverse fault lifted the Permian Ruteh limestone in its hangingwall onto the Ghalemoran Formation (Fig. 3c–e). Post-Cretaceous thrusts (Berra et al. 2007; Zanchi et al. 2009) break along the hinges of several folded layers of the Santonian Ghalemoran Formation (Fig. 3f).

Structural analysis

Folds

Our geometrical analyses of folds and their attitudes enable recognition of the characteristics of a transpression zone. We collected mesoscopic structural data at 25 sites. Diagrams in Fig. 4 summarize the attitudes of folds over the whole study area, while Fig. 5 summarize those of faults, bedding and cleavage. The coexistence of folds and simple shear-related structures in the same area can be attributed to the effect of deformation partitioning (Dabo et al. 2008; Curtis et al. 2010; Dabo and Aïfa 2013). Fold axes and poles to fold axial surfaces concentrate around the circumference of equal-area lower hemisphere Schmidt nets (Fig. 4a, b). Applying Kuiper et al.'s (2011) diagram to these data indicates that pure shear deformation dominates over simple shear deformation in the study area. The average plunge and direction of fold axes in the study area are 10° and 225°, respectively (Fig. 4a, b). If the bedding is assumed to have been horizontal before any deformation, we can combine Fleuty's diagram (1964) with the strain triangle proposed by Jones et al. (2004) to analyse the transpression. In this new graph (Fig. 4c), horizontal and vertical axes correspond to the dip of the fold axial surface and the plunges of fold axes, respectively. Recumbent, upright and vertical folds coincide with dip-slip, contraction and strike–slip vertices. Most of the folds we studied have upright to steeply dipping axial planes that sub-parallel the mean foliations (Fig. 4c) and Class 2 (similar type) in Ramsay's (1967) classification; the folds have sub-horizontal to moderately plunging axes (Fig. 4d). The axial surfaces to folds in transpression zones rotate towards parallel to the shear zone boundaries (Tikoff and Paterson 1998; Fossen et al. 2013; Frehner 2016) which in our case are inclined. This is confirmed herein that the strain path of the folds we studied indicates strain components varying from contraction in the footwall of the nappe (SE) to strike–slip nearer the Talanbar thrust (NW).
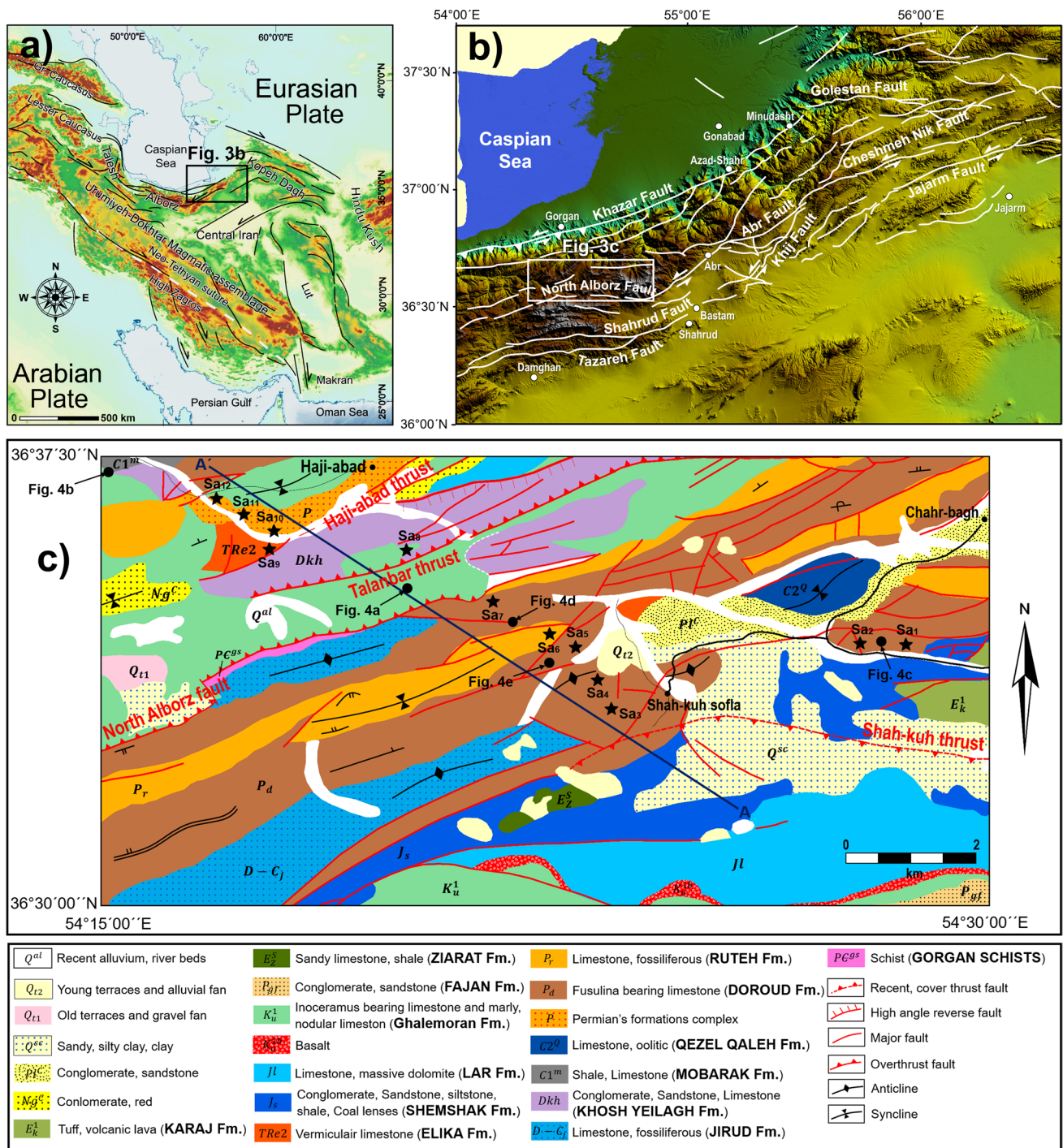
Fig. 2 a Simplified map of Iran showing the distribution of major faults. The *rectangle* indicates the study area (**b**), which is located south of Gorgan County; **c** geological map of the Neka Valley. Position of the study samples and nappe is shown with Sa and filled *stars*, respectively. This map is part of the 1:250,000 Gorgan quadrangle map from Shahrabi (1990). TZB1, TZB2, TZB3 and TZB4 show north-west towards south-east transpressional zone boundaries, respectively. *White dashed line* between Ghalemoran and Khosh Yeilagh Formations show the Late Cretaceous unconformity. Cross section A–A′ is shown in Fig. 9a

Faults

The major faults in the study area are the Haji-abad, Talanbar, North Alborz and Shah-kuh faults (Fig. 2). The

Haji-abad fault passes south of the village of Haji-abad. This thrust fault strikes north-east–south-west, dips 30°–40° NW and implies south-east-directed tectonic transport of the Permian limestones onto Upper Cretaceous units.
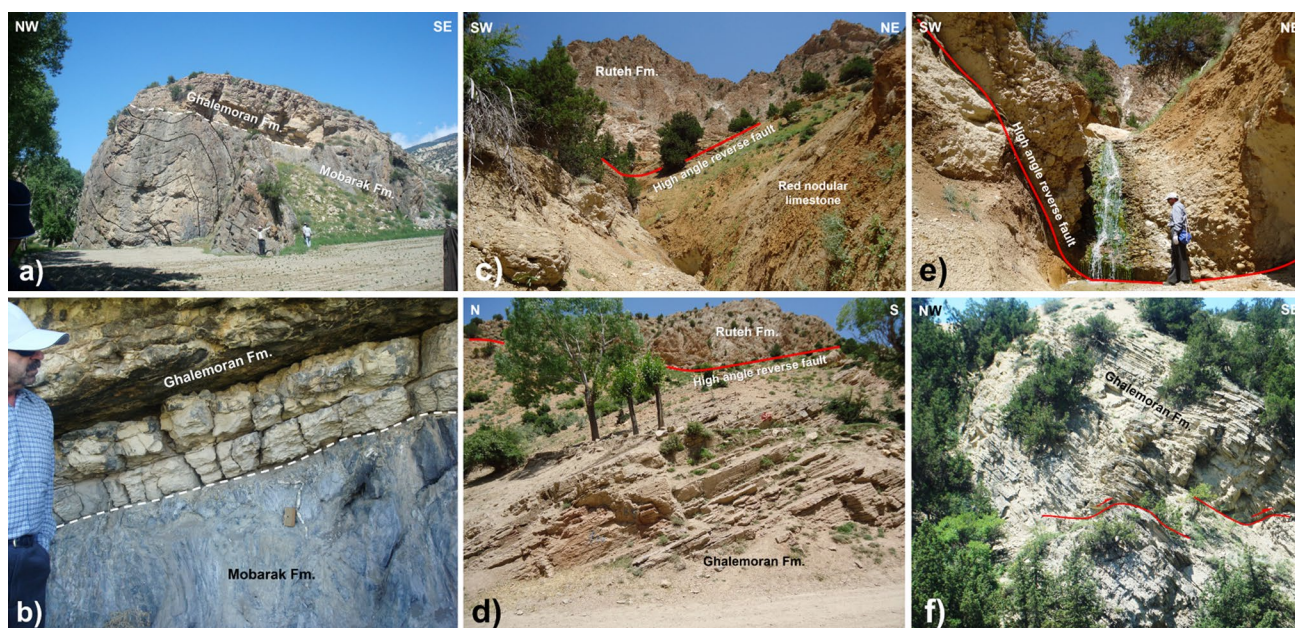
Fig. 3 a, **b** Close views of the Upper Cretaceous unconformity, where the Ghalemoran Formation covers the Mobarak Formation by the flat geometry of the surface. **c–e** A Tertiary high-angle reverse fault is responsible for the uplift of the Permian Ruteh Formation along the hangingwall above the Ghalemoran Formation, which formed the fault scarp. **f** Post-Cretaceous thrusts along the hinge of folded layers of the Santonian Ghalemoran Formation

The Talanbar thrust fault to the south-east dip between 30° and 40° to the north-west and emplaced Upper Devonian units onto the Upper Cretaceous limestones. The Shah-kuh thrust fault on the northern slope of the Kahkashan and Gavkoshan Mountains dips 30°–40° SE and implies north-directed transport. The Shah-kuh thrust strikes east–west to north-east–south-west and carried the Shemshak Formation northward onto the Karaj and Doroud Formations. Quaternary deposits bury the Shah-kuh thrust in the west of the study area.

The reverse or thrust kinematics of most of the faults repeated many formations. The fault data analysis used in this study is dynamic. Our dynamic analysis here refers to the numerical technique developed by Angelier and Mechler (1977), which uses the dihedral grid method to analyse fault slip data. A fault plane and a plane perpendicular to the fault/slickenline intersection divide 3D space into four dihedra, where two are in compression (P, pressure) and two are in extension (T, tension) at the time of faulting (Angelier and Mechler 1977; Angelier 1989). The maximum principal stress (σ_1) lies within P quadrants, and the least principal stress (σ_3) falls within the T quadrants. The $P–T$ dihedral method is a graphic method based on the assumption that all faults moved independently of each other within the same stress field. In the $P–T$ dihedra method, lines bisecting the P and T dihedra along the movement plane estimate the greatest and least principal stress directions. These lines are plotted on the lower hemisphere of an equal-area stereonet, and the principal stress orientations are found by density contouring of the poles to faults to constrain the principal stress axes (Angelier 1989). Such fault analyses in the study area suggest a compressional regime with a NW–SE trending σ_1 axis (P axis in Fig. 5d, e). The P and T axes analyses (Fig. 5a–f) indicate small sinistral strike–slip displacements.

Cleavage

A sub-horizontal to moderately dipping composite cleavage (Fig. 5g) is axial planar to the bedding folded by major F1 recumbent nappes (Fig. 5h) (e.g. Curtis 1998; Curtis et al. 2010). The poles to the original depositional layering or bedding are now folded into a vertical N–S girdle in Fig. 5h. The N–S spread of the poles to the early axial plane cleavage implies folding about steeply dipping axial planes. According to Kuiper et al. (2011), the presence of a cleavage (as in Fig. 5g) oblique to the axial plane probably indicates refraction of a simple shear component during the deformation. This cleavage is axial planar to F1 folds, and the F2 axes do not parallel this cleavage. As the F1 cleavage is folded, its poles do not lie in a straight plane. The sub-horizontal pole to the N–S girdle (Fig. 5h) is the F2 fold axis. Where the cleavage displays the same dip over large areas, it reveals the sense of simple shear of the rock pile.
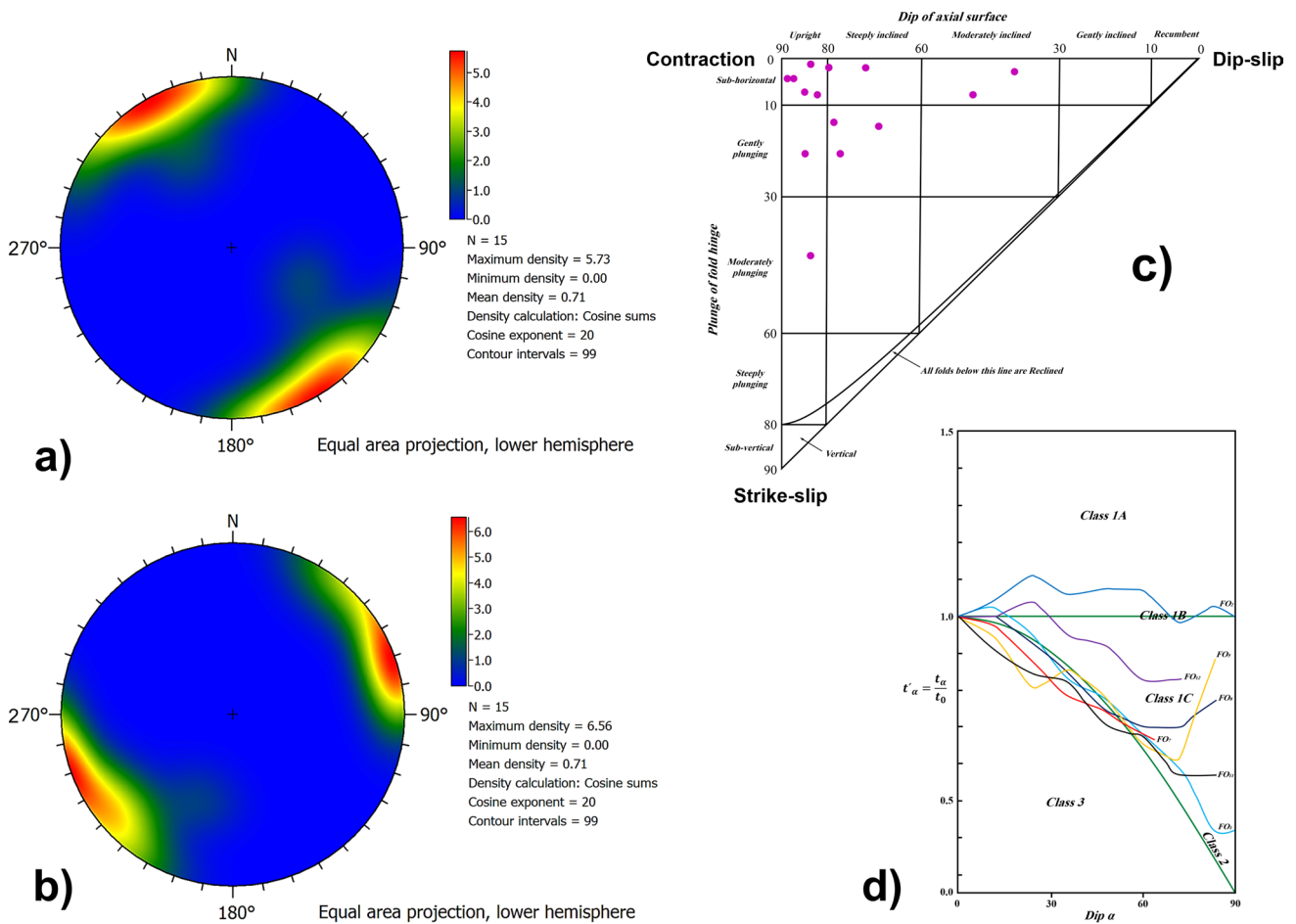
Fig. 4 a Equal-area lower hemisphere projection, stereographic projection of poles to folded bedding planes; **b** stereographic projection of trend and plunge of fold axes; **c** fold attitudes in study area. Note that this diagram is a combination of Fleuty's (1964) and Jones et al.'s (2004) diagrams. **d** Ramsay's (1967) classification of some studied folds

Strain analysis

Sampling and finite strain analysis technique

Finite strains were determined from twelve oriented samples collected from different locations (Fig. 6) and formations (identified in Fig. 2c by star symbols, and listed in Table 1). In all samples, the macrofossils are slightly to moderately more competent than their matrices. The principal axes were measured directly on the specimen using a hand-lens that magnified 10 times. Some pressure solution occurred around most borders, and the foliation in the matrix typically diverted around the markers.

The samples were cut in the principal strain planes to expose the strain ratios (R_{XY}, R_{YZ} and R_{XZ}) so the equation: $R_{XZ} = R_{XY} \cdot R_{YZ}$ applies. The method was applied to enlarged photographs taken of *XY*, *YZ* and *XZ* sections, assuming that the pole to the foliation represents the *Z* axis

and that the stretching lineation parallels the *X* axis. The strain ratios (R_{XY}, R_{YZ} and R_{XZ}) and other strain parameters were then calculated for each sample. The deformed samples come from the Permian carbonate margin succession and were characterized by some alternations of the fusulina and oncoide in fine-grained limestone packstones 50 cm thick. The 2D shapes of relics of fusulina and ooids on XY and XZ surfaces are flattened in the $X/Y = 1–2$ on foliation plane and elongated $X/Z = 2–4$ parallel to the grain shape orientation lineation. Presuming that the ooids began as spheres, and that no volume change occurred, the average strain magnitudes ($R_{XZ} = 2.32$) were calculated from the little to moderately deformed elliptical outlines of the deformed markers. Ooids show core-mantle zones (some have double-layered mantles) of fine-grained calcite and dolomite on *XY* and *XZ* strain surfaces. The three-dimensional shapes of the ooids and fusulina are estimated (Fig. 7a; Table 2). Most mantles of the deformed ooids are
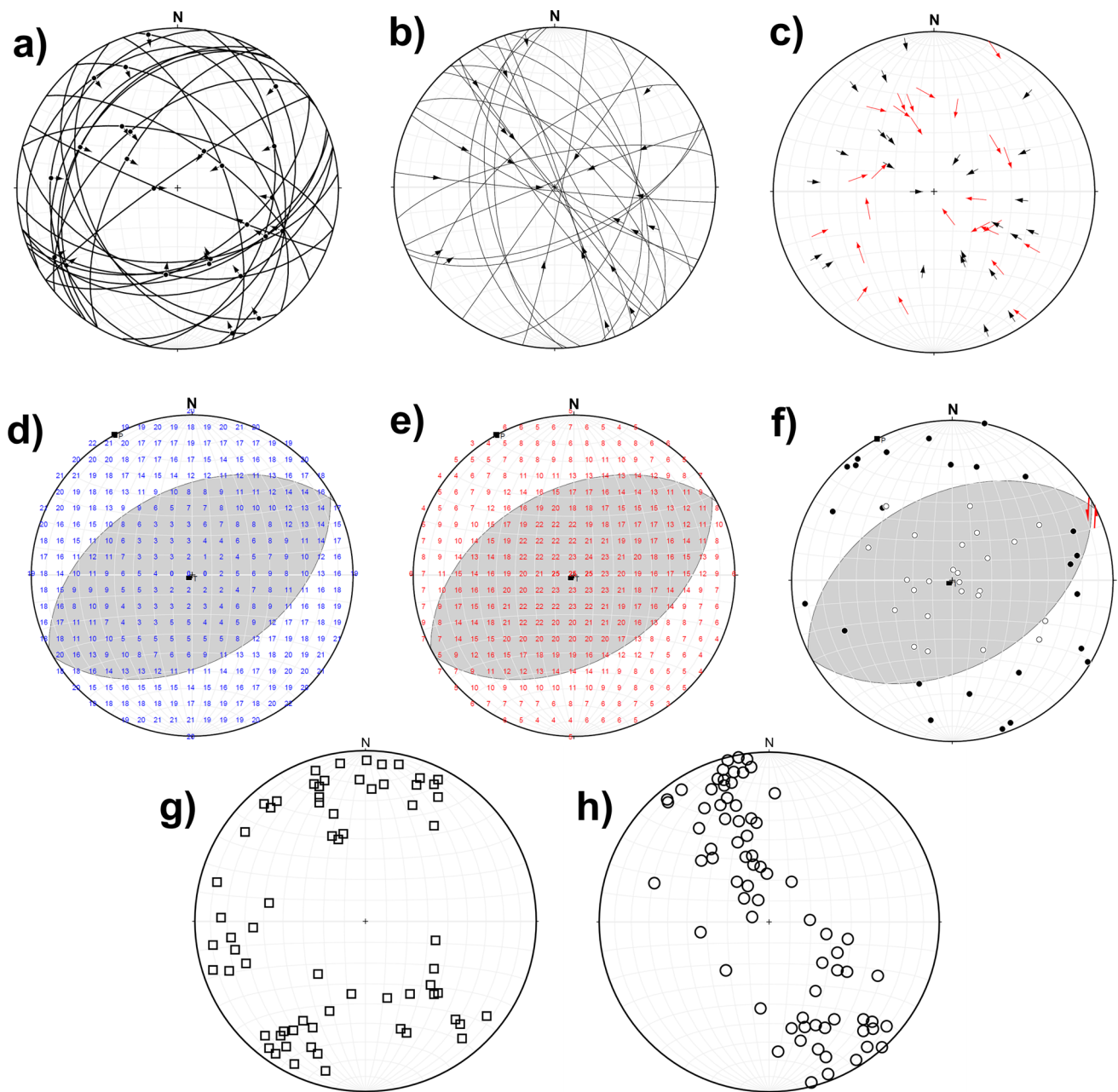
Fig. 5 Equal-area lower hemisphere stereographic projection of **a** fault planes and slickensides (*dots*) with footwall slip direction (*arrows*); **b** movement planes; **c** slip direction (*black arrows*) and tan-gential slickensides (*red arrows*); **d**, **e**, **f** the kinematics *T* (*blue*) and *P* (*red*) axes of the faults; **g** poles to axial plane cleavage; **h** poles to bedding

somewhat thicker in the elongation direction and thinner in the shortening direction.

The Ghalemoran units consist of relatively small, ellip-tical or sub-elliptical objects embedded in mainly biomic-ritic, glauconitic and nodular sandstone or limestone. Most of the macrofossils in the inoceramous-bearing limestones of the Ghalemoran Formation were examined in two-dimensions. In soft, pale argillaceous limestones, their outer layers can be seen under the microscope to

be composed of aggregates of pseudo-hexagonal calcite prisms.

In general, the bulk strain was determined by apply-ing the Fry method (1979) to the inoceramid shells (e.g. González-Casado et al. 2003). The deformed lime-stones usually exhibit $S > L$ fabrics with the planar cleav-age defined by flattened and/or elongated clasts or fos-sils. Figure 7c–k and Tables 1 and 2 show the results of using the Fry Plot Program (Roday et al. 2010; http://
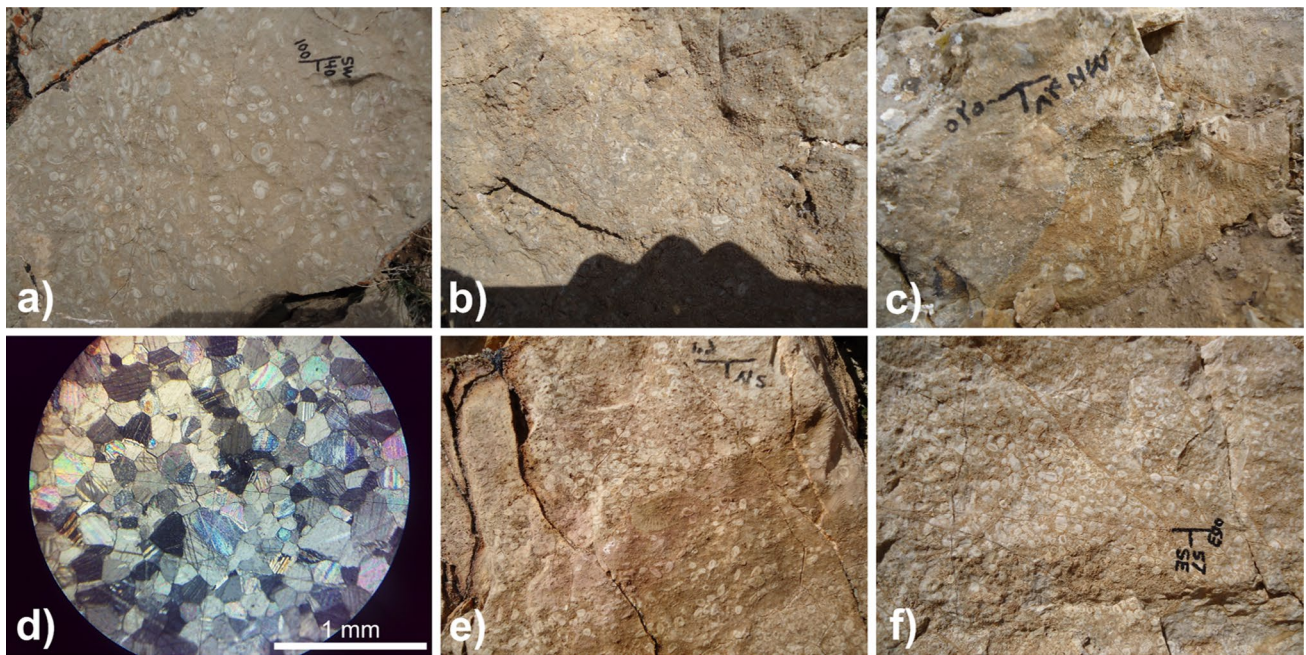
Fig. 6 Some of the studied deformed fossil specimens. **a–c** Weakly to moderately deformed ooid and fusulina bearing limestone samples from Doroud Formation in different locations (Sa$_1$, Sa$_2$, Sa$_4$, Sa$_7$); **d** microscopic view of the calcite part of the inoceramous of Ghalemo-ran Formation (Sa$_8$). Twinned objects are randomly distributed; **e**, **f** weakly deformed limestone samples from Permian complex (Sa$_{10}$, Sa$_{12}$)

Table 1 Strain parameters calculated from deformed samples

Sample	Formation	Dist. (m)	R_{XZ}	R_{XY}	R_{YZ}	k	γ	α	θ'	W_k
1	Doroud	11,000	2.95	1.45	2.03	0.43	1.21	0.88	9	0.51
2	Doroud	10,700	3.07	1.446	2.12	0.4	1.29	0.9	6	0.4
3	Doroud	6640	2.75	1.434	1.91	0.48	1.09	0.9	10	0.55
4	Doroud	6200	2.6	1.45	1.7	0.64	1.02	0.87	12	0.58
5	Doroud	3250	2.5	1.453	1.71	0.64	0.95	0.87	13	0.6
6	Ruteh	2670	2.43	1.45	1.67	0.67	0.88	0.89	15	0.71
7	Doroud	1080	2.15	1.431	1.6	0.71	0.78	0.98	18	0.77
8	Ghalemoran	55	2.1	1.44	1.45	0.98	0.62	0.94	18	0.76
9	Elika	2445	2.05	1.444	1.41	1.08	0.68	0.93	20	0.85
10	Permian complex	2300	2.69	1.451	1.85	0.53	1.05	0.88	11	0.6
11	Permian complex	2630	2.51	1.45	1.73	0.64	0.95	0.87	13	0.65
12	Permian complex	3100	2.77	1.447	1.9	0.5	1.09	0.94	11	0.6

fry-plot-program.software.informer.com/). Input data were manually entered by clicking on a picture of the sample the centre of each object. This program approximates markers with complex shapes as ellipses and automatically plots the centre points of "nearest neighbour" markers and then extracts such strain data as the ellipticity ratio of the principle axes of the bulk ellipse. The length of tie lines joining ellipse centres is plotted against their orientations relative to a chosen reference direction. The distances between particle centres must be at least twice the particle radius (2*r*). Each centre point has six near neighbours at distance 2*r*.

Around each centre, there are also six particles at a distance $2\sqrt{3}r$ (Fig. 7a, b) (Fry 1979; Ramsay and Huber 1983). The output is a plot of dots with a vacancy in the middle. If this vacancy is elliptical, it represents the sectional strain ellipse, if the populations of measured markers deformed homogeneously with an original random distribution. The least-square best-fit ellipse and strain ratios were used for each marker outline.

In many aggregates, these points define an elliptical void and parallel outer ellipse of moderate to high point density around the origin of the overlay. These ellipses have
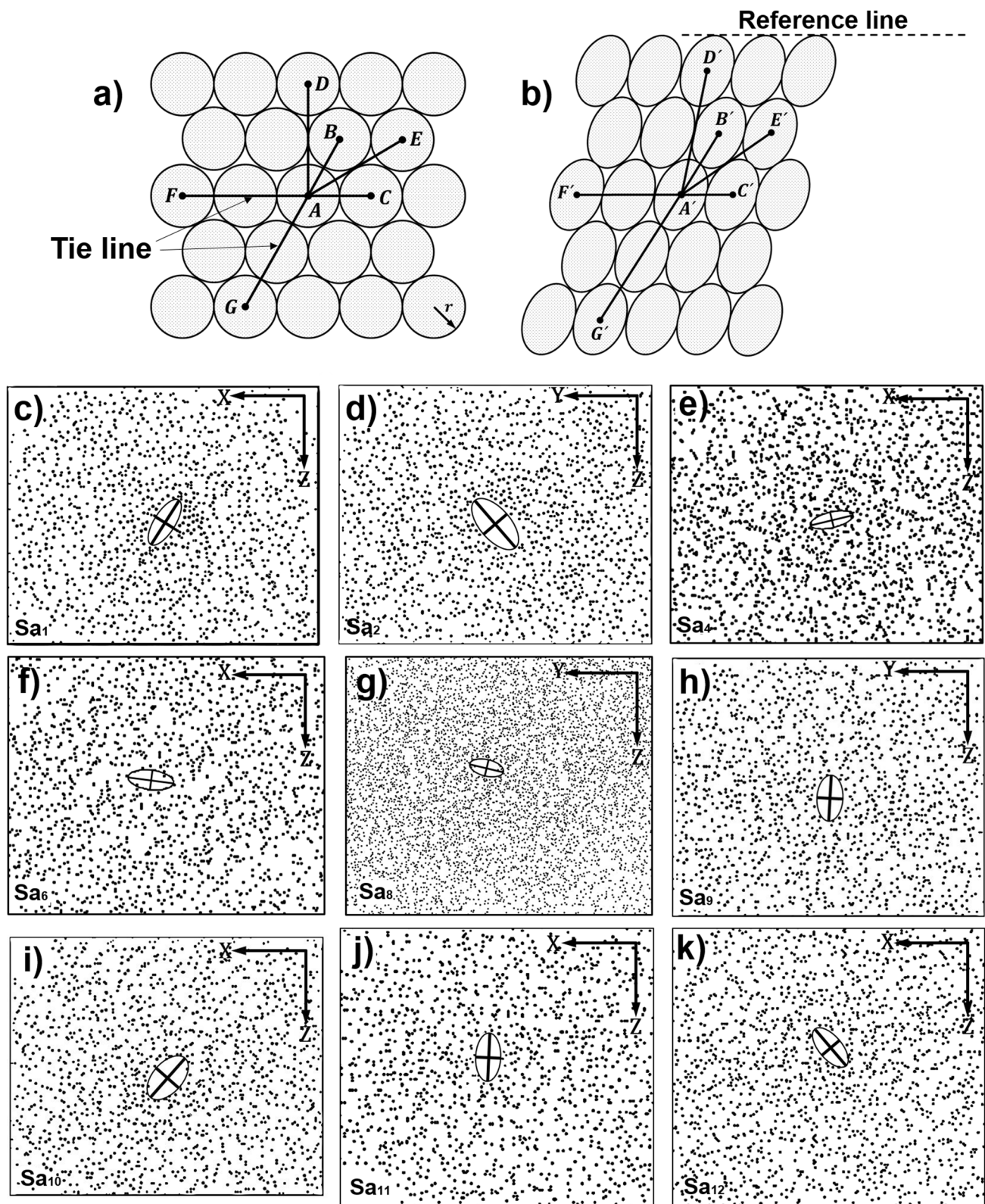
Fig. 7 Geometrical figure of a series of **a** undeformed and **b** deformed circular objects with a radius equal to *r*. Diagram illustrating the principle of the Fry's method (Ramsay and Huber 1983); **c–k** *YZ* and *XZ* planes of finite strain ellipsoid derived from *XY* and *XY* sections using nearest neighbour centre-to-centre Fry's method. Sa_1, Sa_2, Sa_4, Sa_6, Sa_8, Sa_9, Sa_{10}, Sa_{11} and Sa_{12} represent sampling section numbers along the hangingwall block of Shah-kuh thrust to hangingwall block of Talanbar thrust. The finite strain *ellipse* shows elliptical rims surrounding central vacancies, yielding high-resolution ellipses

Table 2 Stretch amounts in the X, Y and Z directions

Sample	X	Y	Z	ln X/Z	ln Y/Z	ln X/Y	K	D	ν	ε_s
1	1.623	1.12	0.55	1.081	0.71	0.37	0.52	0.8	0.31	0.775
2	1.65	1.14	0.53	1.121	0.752	0.368	0.5	0.83	0.33	0.808
3	1.58	1.1	0.57	1.011	0.65	0.36	0.55	0.74	0.29	0.724
4	1.59	1.07	0.53	0.953	0.582	0.371	0.64	0.65	0.21	0.679
5	1.53	1.05	0.61	0.913	0.538	0.373	0.69	0.65	0.18	0.648
6	1.52	1.05	0.62	0.884	0.513	0.37	0.72	0.63	0.16	0.627
7	1.44	1.01	0.68	0.764	0.405	0.358	0.88	0.59	0.06	0.54
8	1.44	1.00	0.69	0.735	0.37	0.364	0.98	0.52	0.01	0.519
9	1.63	1.13	0.54	0.713	0.346	0.367	1.06	0.5	-0.03	0.504
10	1.57	1.08	0.58	0.988	0.616	0.372	0.6	0.72	0.25	0.705
11	1.54	1.06	0.61	0.919	0.548	0.37	0.67	0.66	0.2	0.653
12	1.59	1.1	0.57	1.011	0.641	0.369	0.57	0.74	0.25	0.723

the same shape of the finite strain ellipse for homogeneously deformed populations of originally statistically uniform centres. The simplicity and elegance of Fry's method have encouraged its application to a wide range of rocks, although it requires that the original objects began with a random non-Poisson distribution. High-resolution ellipses are found from markers of uniform size that have been deformed homogeneously (Fry 1979; Roday et al. 2010). The results are summarized in a logarithmic Flinn diagrams (Ramsay and Huber 1983) (Fig. 8a). Software, methodologies, distribution of markers in the section, and differences in the number of markers in the section account for slight difference between the results and concentration of points on the elliptical rim.

Strain parameters

The three axes of the strain ellipsoid ($X \geq Y \geq Z$) were determined from two-dimensional measurements on three mutually perpendicular surfaces. We used the Ramsay's (1967) logarithmic diagram with $\ln(Y/Z)$ along the abscissa and $\ln(X/Y)$ along the ordinate axis (Fig. 8a). According to Hossack (1968), this classification is called the strain symmetry. The strain geometry is identified with the Flinn K value (Eq. 1), which is >1 for apparent constrictional ellipsoids, 1 for plane strain and <1 for apparent flattening ellipsoids. In turn, to evaluate the amount of deformation or strain intensity, we calculated the D value (Eq. 2), as a measure of the distance from the origin on the Ramsay's diagram (i.e. a measure of the amount of strain):

$$K = \frac{\ln(R_{XY} - 1)}{\ln(R_{YZ} - 1)} \tag{1}$$

$$D = \sqrt{\ln(R_{XY})^2 + \ln(R_{YZ})^2} \tag{2}$$

In addition, the finite stretches S_X, S_Y and S_Z, which are parallel to the principal axes X, Y and Z, respectively, are derived using the following equations (e.g. Kassem and Abd El Rahim 2010; Kassem 2011, 2014):

$$S_X = R_{XY} \times S_Y \tag{3}$$

$$S_Y = \sqrt[3]{R_{XZ} / R_{XY}^2} \tag{4}$$

$$S_Z = {S_Y}/{S_X}. \tag{5}$$

Results of finite strain analyses

Strain symmetry

The shapes of all the strain ellipsoids measured by the Fry method are shown in Fig. 8a and Table 2. All but three of the samples plot in the apparent flattening field ($K = 0.5–0.69$). Flinn's parameter k is in Table 1. Modified Flinn's parameter by Ramsay K is in Table 2). Three samples plot near the plane strain line, on the apparent flattening field (sample 7, $K = 0.88$), on the apparent constriction field (sample 9, $K = 1.06$) or on the line (sample 8, $K = 0.98$); D values range from 0.5 to 0.83 although samples 7, 8 and 9 show lower values ($D = 0.5–0.59$) than the apparent flattening samples ($D = 0.65–0.83$). In addition, all these samples plot in field 2 (field of extension/contraction) and its transpression sub-field in Ramsay's two-dimensional strain field diagram (1967) (Nabavi 2012). Referring to Ramsay's two-dimensional strain field diagram (1967), a strike–slip component of shear develops approximately along the pure shear/simple shear strain path. Such intermediate types of tectonics regimes as transpression and transtension lie in the corresponding sub-field of field 2, so that all strain paths with a strike–slip component indicate transpression and all strain paths above this line indicate transtension (Fig. 8b) (Milnes 1994).

The variations in K and D values (Fig. 8a) reflect the heterogeneous nature of the deformation that ranges from
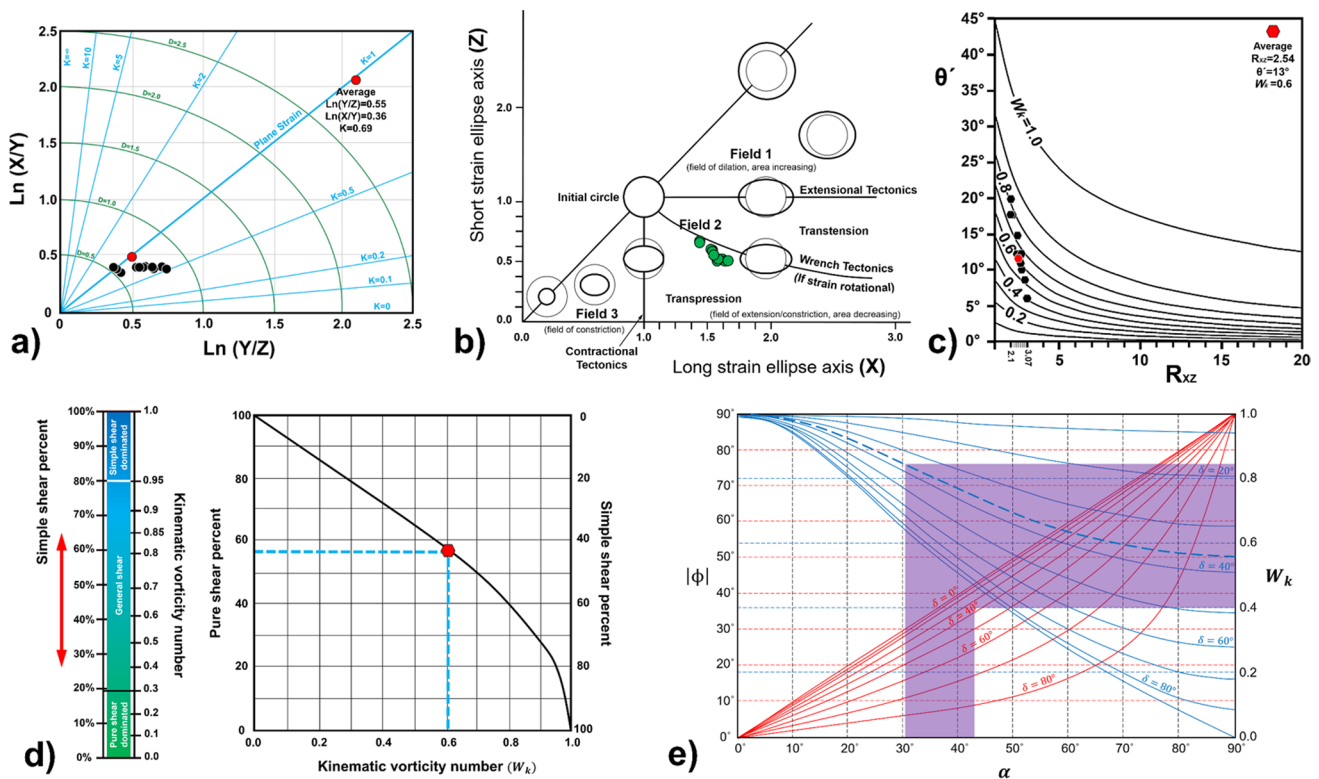
Fig. 8 a Ramsay logarithmic diagram showing relative strain or strain symmetry as obtained by Fry analysis shown by *black dots*. The plotted data show K values <1, which is characteristic of an oblate triaxial ellipsoid. The average K value is marked as a *red circle*. **b** Strain data from the Neka Valley plotted in Ramsay's strain field diagram (1967) to characterize the tectonic regime (Nabavi 2012). **c** *Plot* showing the finite strain ratio R_{XZ} versus angle θ' for estimate of W_k in the study area (Tikoff and Fossen 1995). The aver-

age value of W_k is 0.6 and is marked as a *red hexagonal*. **d** Diagram showing the nonlinear relationship between the average kinematic vorticity number (W_k) and components of pure and simple shear for instantaneous 2D flow (Law et al. 2004) on which the obtained value of W_k for the study area is plotted. **e** α versus ϕ and W_k for different dip values of shear zone (δ) (from Díaz-Azpiroz et al. 2014). Combination of ϕ and W_k yielding a fair-to-good fit in resulting angle α for study area (*violet*) is shown

approximately simple shear to non-coaxial flattening strain (e.g. O'Hara 1990; Talbot and Sokoutis 1995; Capponi et al. 2003; Kassem and Ring 2004; Tripathy et al. 2009; Kassem and Abd El Rahim 2010; Kassem 2011; Kassem et al. 2012; Talbot 2014). Liu et al. (1995) defined a parameter K to measure the degree of obliquity partitioning; $K = 0$ and $K = 1$ are two end-member cases of no obliquity and complete obliquity partitioning, respectively. Our average of $K = 0.69$ indicates intermediate obliquity partitioning. There is no lineation when $K = 0$, and there is a very strong lineation when $K = \infty$. In practice, a lineation may not have any visible petrographic expression when K is below a certain critical value, e.g. 0.3 or 0.4 (Robin and Cruden 1994).

Finite stretches

The finite stretches are presented in Table 2. S_X ranges from 1.44 to 1.65, S_Y from 1 to 1.14 and S_Z from 0.53 to 0.69 (Table 2). The latter indicates a 31–47 % shortening.

Kinematic vorticity number (W_k)

Vorticity describes how fast a particle rotates in a softer medium during ductile flow (Xypolias 2010; Fossen 2016). The kinematic vorticity number (W_k) measures the degree of non-coaxiality (the relative contribution of rotation and stretching) involved in progressive deformation histories. It also relates the effects of rotation of material lines (relative to non-material maximum instantaneous stretching axes, ISA$_{max}$) and of stretching of these material lines (Means et al. 1980; Passchier 1987; Wallis 1992, 1995; Xypolias 2010; Mulchrone 2013). $W_k = 0$ indicates pure shear, 1 simple shear, any value in between sub-simple shear, and larger than 1 super-simple shear (Means et al. 1980; Fossen and Tikoff 1993; Passchier and Trouw 2005; Fossen 2016). Several methods have been proposed for constraining the kinematic vorticity number in natural rocks. Figure 8b uses the R_{XZ}/θ'-method (Tikoff and Fossen 1995; Xypolias 2010), where θ' is the angle between the long axis of finite

strain ellipsoid and the deformation zone boundary. W_k can be obtained when R_{XZ} and θ' are known.

Because our strain data are incomplete, we have to make some assumptions to define the geometry of the deformation zone boundaries. The north-western (TZB1 and TZB2 in Fig. 2c) and south-eastern boundaries (TZB3 and TZB4 in Fig. 2c) of the study area coincident with the Haji-abad, Talanbar, and minor branches of the North Alborz, and Shah-Kuh thrusts, respectively. The average strike of these thrust faults at N50°E was taken as our reference line, W_k on the graph of R_{XZ}/θ' (Xypolias 2010). The mean values of R_{XZ} and K in the study area are 2.54 and 0.69, respectively (Fig. 8a). Therefore, the angle of θ' from strain, P and T dihedral method of thrusts and geometrical analysis of folds with respect to reference lines is constrained to lie between 6° and 20° (average = 13°). Hence, the W_k values lie in range of 0.4–0.85 (average = 0.6) (Fig. 8c). These W_k values indicate 35–71 % pure shear and 29–65 % simple shear for the total deformation in the study area. The average W_k values revealed 59 % pure shear and 41 % simple shear (Fig. 8d). These values suggest a mainly pure shear-dominated transpression (Fossen et al. 1994), as expected for compressional tectonic settings (Mukherjee and Koyi 2010).

Kinematic modelling

The dip (δ) and strike (β) (the angle in the horizontal plane between the boundary of a transpression zone and its direction of overall shortening) affect both the shape of the finite strain ellipsoid and its orientation (e.g. Sanderson and Marchini 1984; Jones and Tanner 1995). Progressive deformation can be modelled by substituting the amount shortening across the zone (S) measured parallel to the far-field displacement vector. This allows the progressive change in shape of the finite strain ellipsoid to be plotted on a Flinn diagram. Meanwhile, the progressive rotation of the ellipsoid axes can be plotted on stereonets (Jones et al. 2004). The dip of our zone is difficult to constrain from our regional data. We therefore used the average dip of the bounding faults as the dips of the deformation zone boundaries. Hence, the Haji-abad and Shah-Kuh thrusts, which are the main boundaries, indicate that the dip of the zone is 37° and its strike is 050°. Analysis of the compressional direction in the study area nappes (Fig. 5a–f) by kinematic analysis and the P and T dihedra method shows that they were shortened along a N50°W–S50°E axis (Nabavi 2012); hence, the β angle is 80°. The north-western zone

boundary coincides with the Talanbar thrust (TZB2 in Fig. 2c). The Haji-abad thrust (TZB1 in Fig. 2c) and the south-eastern zone boundary coincide with the reverse/thrust faults between Ghalemoran and Doroud/Ruteh Formations (TZB3 in Fig. 2c). These boundaries extend along strike to the sinistral strike–slip fault North Alborz faults due to inclined transpression in the intervening nappes.

It is noteworthy that the entire study area is a transpressional zone involving four major thrusts separating individual nappes. From north to south, these are the Haji-abad, Talanbar, minor branch of North Alborz, and Shah-Kuh thrusts (TZB4 in Fig. 2c). Each of these thrusts plays the role of transpressional zone boundaries. The Haji-abad and Shah-Kuh thrusts are the main boundaries of transpressional zone. The Chahar-bagh nappe is another transpression structure in the middle of the main transpressional zone. Its boundaries are the Talanbar and minor branches of the North Alborz thrusts.

In order to determine the deformation matrix of the studied inclined transpression (F) the following relation (Eq. 6 in Davis and Titus 2011) has been used:

$$F = \begin{bmatrix} 1 & \gamma_{xy}\frac{1-\alpha_z^{-1}}{\ln \alpha_z} & 0 \\ 0 & \alpha_z^{-1} & 0 \\ 0 & \gamma_{yz}\frac{\alpha_z-\alpha_z^{-1}}{2\ln \alpha_z} & \alpha_z \end{bmatrix} \tag{6}$$

We cannot apply Jones et al.'s (2004) equation for inclined transpression because three main deformations (strike–slip simple shear followed by dip-slip simple shear followed by orthogonal pure shear) did not act simultaneously and hence did not result in transpression. In the above relations (Eq. 6), γ_{xy} is the simple shear in the XY plane (strike–slip movement) so that $\gamma_{xy} = \tan\psi_{xy}$. The simple shear in the YZ plane is γ_{yz} (dip-slip movement) so that $\gamma_{yz} = \tan\psi_{yz}$. The term α_z parallels the Z axis; the ratio of the deformed to original zone width (measured along the Y axis) is α_z^{-1}. The term ψ_{xy} is the angle between the basal boundary of the deformed zone (which is in the form of a parallelogram in profile) with respect to the (often rectangular) undeformed state. Substituting these values into expression 6 indicates that the acute angle of the transpression base is 80° and accordingly ψ_{xy} is 10° and γ_{xy} is 0.176. According to our calculated strain data, the average of α_z is approximately 0.9. In order to calculate ψ_{yz} and α_z^{-1}, it is necessary to calculate the amount of shortening (S) using the equations: $\alpha_z^{-1} = 1 - S$ and $\tan\psi_{yz} = S.\cot\delta(1 - S)^{-1}$. We calculated the amount of shortening using the equation by Law et al. (2004):

$$S = \left\{ \frac{1}{2}\left(1 - W_k^2\right)^{1/2}\left[\left(R_{XZ} + R_{XZ}^{-1} + 2\frac{\left(1 + W_k^2\right)}{\left(1 - W_k^2\right)}\right)^{1/2} + \left(R_{XZ} + R_{XZ}^{-1} - 2\right)^{1/2}\right] \right\}^{-1} \tag{7}$$
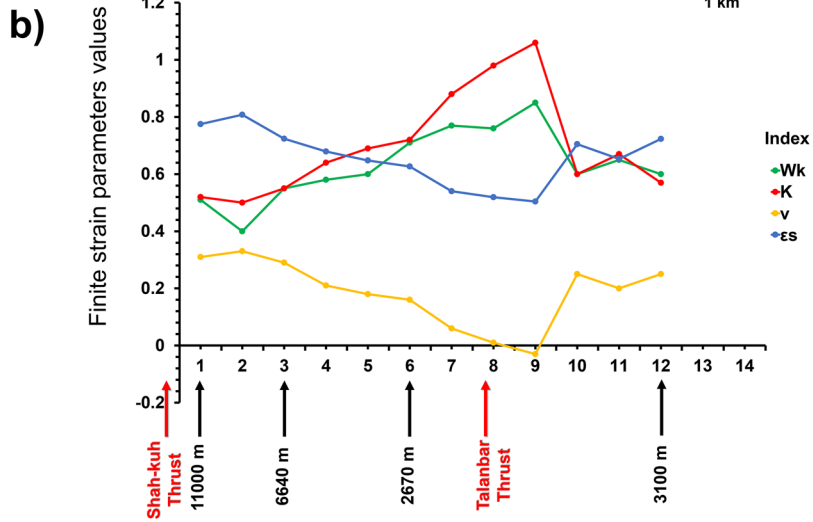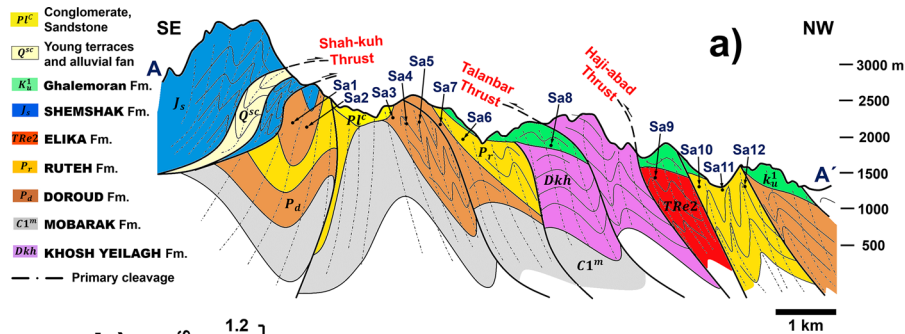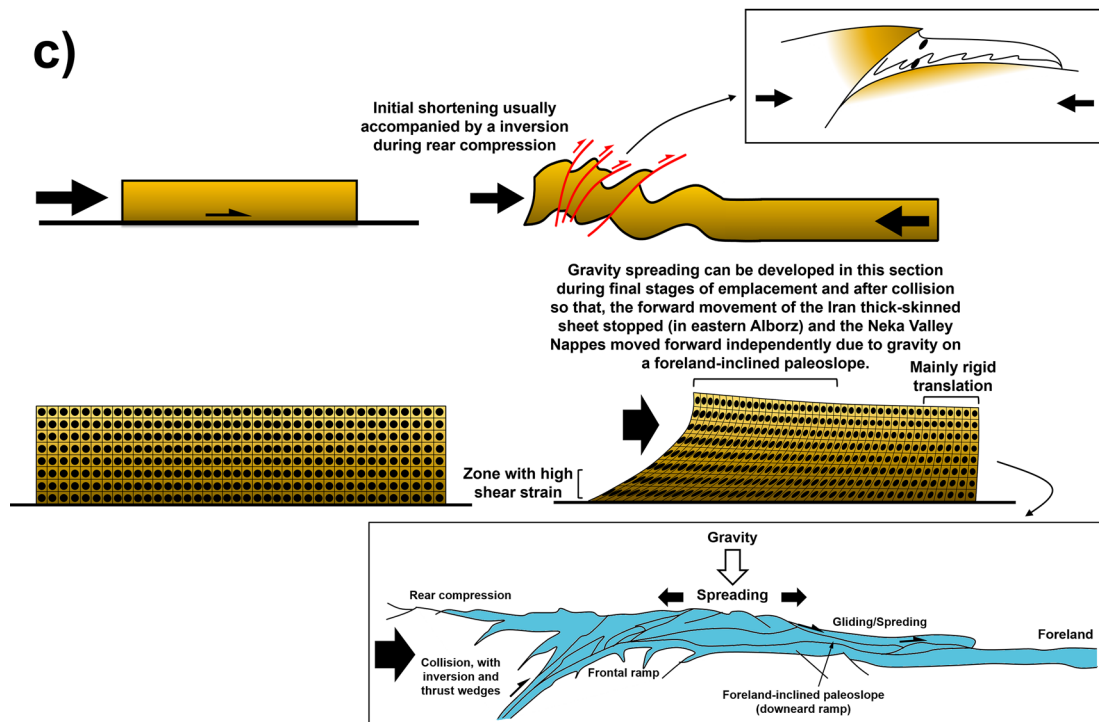
◀**Fig. 9 a** Geological cross section through the study area. The entire area is a transpressional deformation zone bound by the Haji-abad, Talanbar, minor branches of the North Alborz, and the Shah-Kuh thrusts; **b** *plot* showing the spatial variation of strain parameters (K, v, W_k and ε_s) of the respective samples along the cross section and to the relative position from Shah-kuh and Talanbar thrusts; **c** *above*: push from the rear of undeformed configuration on a *horizontal surface*, and deformation through folds and reverse/thrust faults and subsequently rear compression mechanism of nappe emplacement. *Below*: distribution of strain ellipses in rear compression mechanism

Substitution of the average kinematic vorticity number ($W_k = 0.6$) and finite strain $R_{XZ} = 2.54$ in Eq. (7) gives $S = 0.67$. Therefore, $\alpha_z^{-1} = 0.33$ and $\tan\psi_{yz} = 4.0$; so the inclined transpression matrix becomes:

$$F = \begin{bmatrix} 1 & -1.12 & 0 \\ 0 & 0.33 & 0 \\ 0 & -0.12 & 0.9 \end{bmatrix} \qquad (8)$$

According to Provost et al. (2004), Pollard and Fletcher (2005), p. 178, and Davis and Titus (2011), we should use the log sum in exponentials method, which is logarithmic. This uses the velocity gradient tensors (shown by L_1 and L_2) so that the combined velocity field can be taken to be two simultaneous deformations that sum the components velocity fields, i.e. $\exp(L_1 + L_2)$. This method implies that the velocity gradient tensor (L) of the studied inclined transpression is equal to the sum of three matrices Eq. (6), as:

$$L = \begin{bmatrix} 0 & \gamma_{xy} & 0 \\ 0 & -\ln\alpha_z & 0 \\ 0 & \gamma_{yz} & \ln\alpha_z \end{bmatrix} = \begin{bmatrix} 0 & 0.176 & 0 \\ 0 & -0.105 & 0 \\ 0 & 4.0 & 0.105 \end{bmatrix} \qquad (9)$$

Discussion

Variation of strain parameters in space

Transpression results in oblate ellipsoids (in the field of apparent flattening) with vertical X axes for pure shear-dominated transpression and horizontal X axes for strike–slip-dominated transpression (Fossen et al. 1994; Tikoff and Teyssier 1994; Tikoff and Greene 1997; Sanderson 2014; Fossen 2016). Tikoff and Teyssier (1994) concluded that reverse faults are most likely to form and remain active in a transpressional system together with a strike–slip component. This is because it would be difficult for a strike–slip shear zone to accommodate the pure shear component. We assume a similar scenario in the present study of the Neka Valley. According to Dabo and Aïfa (2013), how the shapes (flattening, constriction or plane finite strain) of the finite strain ellipsoid vary in space, and in our area, implies a partitioning of the deformation. However, strain ellipsoids measure homogeneous flows and cannot by themselves provide information about how the deformation partitioned

until their spatial variations are taken into account. We do that here by plotting strain magnitudes as a function of distance from the major thrust faults along the studied cross section (Fig. 9a). We measured the (irregular) distances in Fig. 9b perpendicular to the thrust faults by Global Mapper software from a satellite image of the area. In the present case, the samples (1–7) and samples (8–12) were collected up to 11,000 and 3000 m from the Talanbar thrust in its footwall and hangingwall blocks, respectively. Note that the Talanbar footwall block also is the footwall block of the Shah-kuh thrust.

Significant variations in the regional finite strain were found along the profile in Fig. 9b. It has been observed that in the Talanbar footwall block between 11,000 m to the reading closest from Shah-kuh thrust, there is a gradual increase in strain structurally up (from SE towards NW) towards the Talanbar thrust. In addition, the strain values increases structurally upward towards the thrust in the Talanbar hangingwall block. A similar pattern has been observed from many thrust sheets in fold-and-thrust belt throughout the world. In general, the strain values represent a periodic pattern from the Shah-kuh thrust to the Haji-abad thrust. Figure 9b therefore shows plane strain near the Talanbar thrust to oblate ellipsoids away from it. This could be due to sinistral strike–slip faulting in the Ghalemoran Formation. From 6640 to 2670 m, towards the Talanbar thrust, there is no significant variation in the strain values. This bulk pure shear is probably due to the nearly constant lithology of the strained rocks and their nearly uniform ductile flow rates (pure shear dominates over simple shear) associated with the Talanbar and Shah-kuh thrusts. Increased strain towards the thrust faults is attributed to the local increase in simple shear near the faults (Ramberg 1975; Abad et al. 2003). The periodic strains down through in the Neka Valley probably indicate the activity of several minor thrusts or minor shear zones we missed in the field (e.g. Bauer et al. 2011). Alternatively, they could indicate superposed phase of thrusts.

Sinistral transpression and strain partitioning

Our estimated W_k values reflect spatial strain partitioning into both coaxial and non-coaxial deformations across the study area. A relationship exists between the regional kinematic vorticity number imposed by plate motion within the zone of distributed deformation and the percentage of shear displacement beside local discrete shear zones. For plate motion dominated by moderately oblique convergence, W_k of the transpressional zone decreases quite linearly with increasing partitioning of the strike–slip component (Fossen et al. 1994; Tikoff and Teyssier 1994; Jones and Tanner 1995). The occurrence of contemporaneous strike–slip and dip-slip deformation (oblique 3D deformation) with a
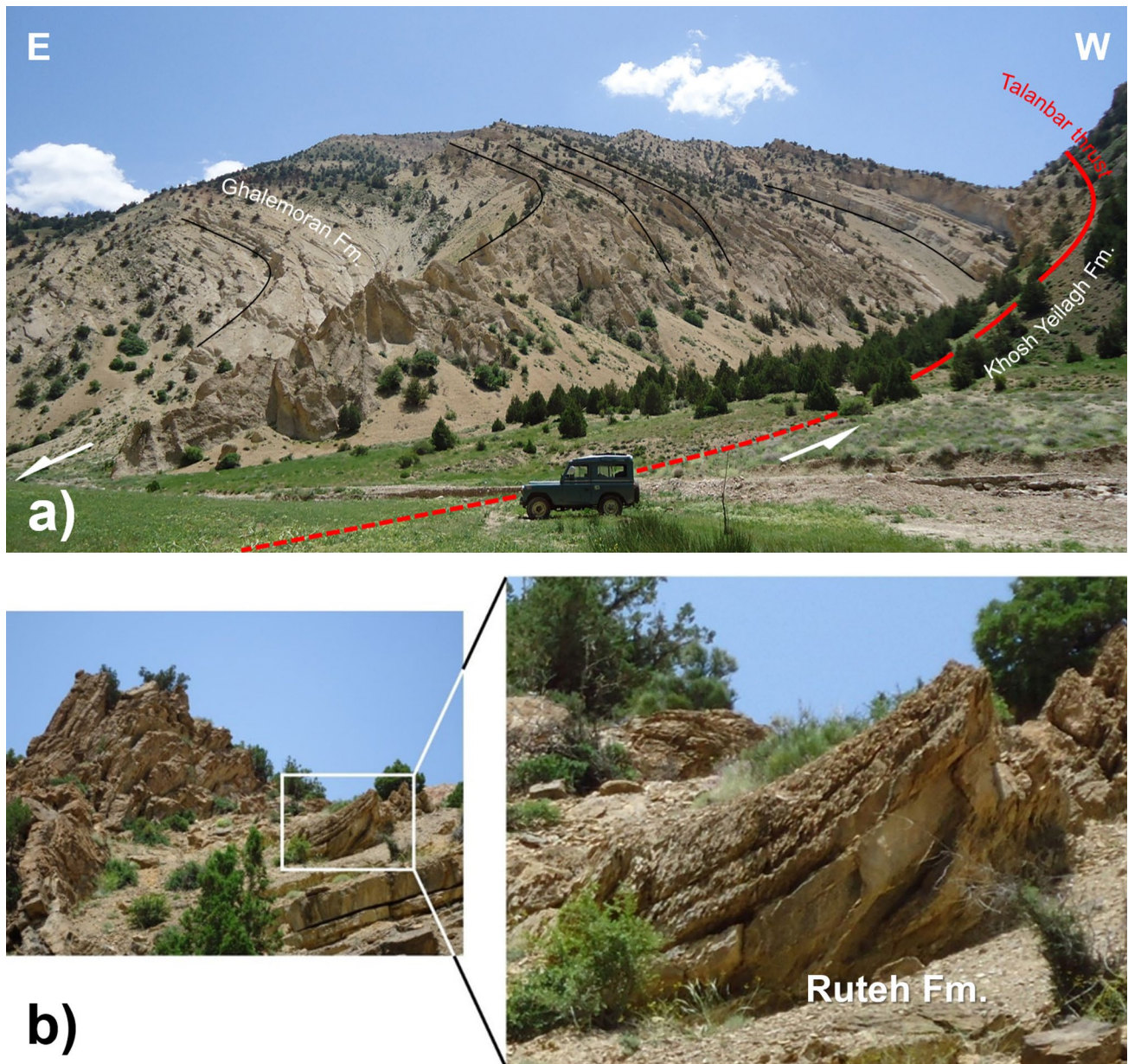
Fig. 10 a Sinistral strike–slip faulting with Talanbar thrust (shown as *red dashed line*) along Khosh Yeilagh and Ghalemoran formations boundary. **b** Approximately, foliations are sub-parallel to axial surfaces of folds in study area and generally are of high angle with respect to the horizon

strong component of pure shear deformation is consistent with a transpression deformation zone. Our average kinematic vorticity number of $=0.6$ reflects general pure shear-dominant transpression (Fossen et al. 1994) in between domains of simple (non-coaxial) shear near the thrusts (e.g. Faghih et al. 2012; Sarkarinejad et al. 2010a, 2012). Natural deformation is commonly heterogeneous, and here we have shown that thrusts partition the general orogenic extrusion of the nappes. Our average value of W_k of 0.6 indicates that the Neka Valley underwent transpressional

deformation involving 59 % pure shear and 41 % simple shear components (Fig. 8d). It also indicates that the continuous deformation in the Neka Valley occurred in a general shear regime. General shear of rocks almost certainly involves the development of secondary shear planes (review in Mukherjee et al. 2012). Strain intensity partitioned from $D = 0.5$ to 0.83 within the transpression zone. Our results in the eastern Alborz are similar to those found by regional studies of both ancient and modern transpression zones worldwide. Like many others, we have found that the

Table 3 Geometrical features of studied folds

Fold	Interlimb angle (°)	Fold axes	Axial surface	Vergence	The fold section	Symmetry	Folding angle (°)	Tightness
1	29	013/038	220/79NW	SE	Semi-cylindrical	Non-symmetrical	151	Tight
2	70	008/071	064/48SE	NW	Semi-cylindrical	Overturned	110	Close
3	85	004/068	068/89SE	NW	Semi-cylindrical	Symmetrical	95	Open
4	47	021/228	053/78SE	NW	Semi-cylindrical	Non-symmetrical	133	Close
5	35	021/231	053/85SE	NW	Semi-cylindrical	Non-symmetrical	145	Close
6	36	045/201	027/84SE	NW	Semi-cylindrical	Non-symmetrical	144	Close
7	92	004/084	084/88SE	NW	Cylindrical	Symmetrical	88	Open
8	82	007/083	083/85SE	NW	Semi-cylindrical	Symmetrical	98	Open
9	90	002/250	070/73SE	NW	Cylindrical	Non-symmetrical	90	Open
10	88	002/072	253/80NW	SE	Cylindrical	Non-symmetrical	92	Open
11	70	014/239	232/67NW	SE	Cylindrical	Non-symmetrical	110	Close
12	94	001/250	241/83NW	SE	Semi-cylindrical	Symmetrical	86	Open
13	98	003/210	206/39NW	SE	Semi-cylindrical	Overturned	82	Open
14	115	008/223	224/82NW	SE	Semi-cylindrical	Symmetrical	65	Open
15	95	000/226	236/84SE	NW	Semi-cylindrical	Symmetrical	85	Open

regional deformation partitions into blocks of largely pure shear separated by narrow zones of simple shear (Iacopini et al. 2007, 2008).

Most strain partitioning appears to be controlled by the presence of mechanical heterogeneities (in particular, boundaries) on any scale, in particular the proximity to weak tract-bounding faults and the presence of lithologically controlled regions of high pore fluid pressures (Jones and Tanner 1995; Curtis 1998; Tavarnelli and Holdsworth 1999; Tavarnelli et al. 2004; Viola and Henderson 2010; Massey and Moecher 2013). Two broad forms of strain partitioning are distinguished in transpression zones based on the spatial and chronological relationship between the boundary-parallel and boundary-normal displacements. These are (a) spatial strain partitioning and (b) temporal strain partitioning. Here, we have used spatial strain partitioning that is defined by Curtis (1993, 1997, 1998) as: "… *the resolved components of the oblique relative motion vector are manifest as synchronous, spatially distinct domains of deformation*". Important in this definition is the cotemporaneous development of lateral contraction-dominated (e.g. folds and reverse faults) and wrench-dominated (e.g. strike–slip faults and ductile shear zones) structures.

Complex 3D strain partitioning patterns are common in the continental crust. They are often related to the kinematics of three-dimensional deformations. Determination of strain-active zone boundaries is approximate and arbitrary; they depend on the scale of study because strain partitioning can occur on any scale. The upright, close to tight chevron folds, moderate to steep dip cleavages, $K < 1$, stretch value less than 1, a change from an approximately constant volume, plane strain coaxial deformation in the upper parts of the study area to non-coaxial flattening strain in basal parts

(i.e. from young to old formations in the study area) and their emplacement to shallower crustal level, the Neka Valley nappes emplaced by rear compression mechanism or push from the rear during two deformation stages, when the sedimentary succession was detached, shortened and transported over the Neka Valley's major thrusts. In addition, gravity spreading and gliding mechanisms could have developed as a result of rear compression mechanism over a horizontal no-slip basal boundary which is marked by frontal rolling and a tank-track fold (Brun and Merle 1985, 1988; Merle 1986; Talbot and Aftabi 2004; Talbot and Pohjola 2009; Baikpour and Talbot 2012; Nabavi 2012; Nabavi et al. in preparation) (Fig. 9c). The deformations in and around the nappes studied here can be partitioned into two spatial strain domains: (1) non-coaxial shortening dominated and (2) sinistral strike–slip dominated. In the first domain, shortening was along a NNW–SSE axis by dip-slip shearing. This domain is characterized by upward-facing upright folds with curved hinges and eroded asymmetric SE verging folds in the Ghalemoran Formation (e.g. like domain 2 in Fig. 12 of Jones et al. 2004). These structures can indicate the beginning of folding (Dubey and Cobbold 1977) of layers inclined to the principle strain axes (Treagus and Treagus 1981). By contrast, the second domain is characterized by sinistral strike–slip faulting close to secondary zone boundaries within inside the major Chahar-bagh nappe (Fig. 10a).

Styles of multilayer folds of different lithologies depend on their thicknesses and competence contrasts (Twiss and Moores 2007). In our study area, parallel open anticlines and chevron folds formed in the Doroud and Elika Formations due to flexural slip folding and with semi-cylindrical, upright to steeply inclined, open folds (with interlimb angle of 85°–115°) about semi-horizontal to slightly plunging
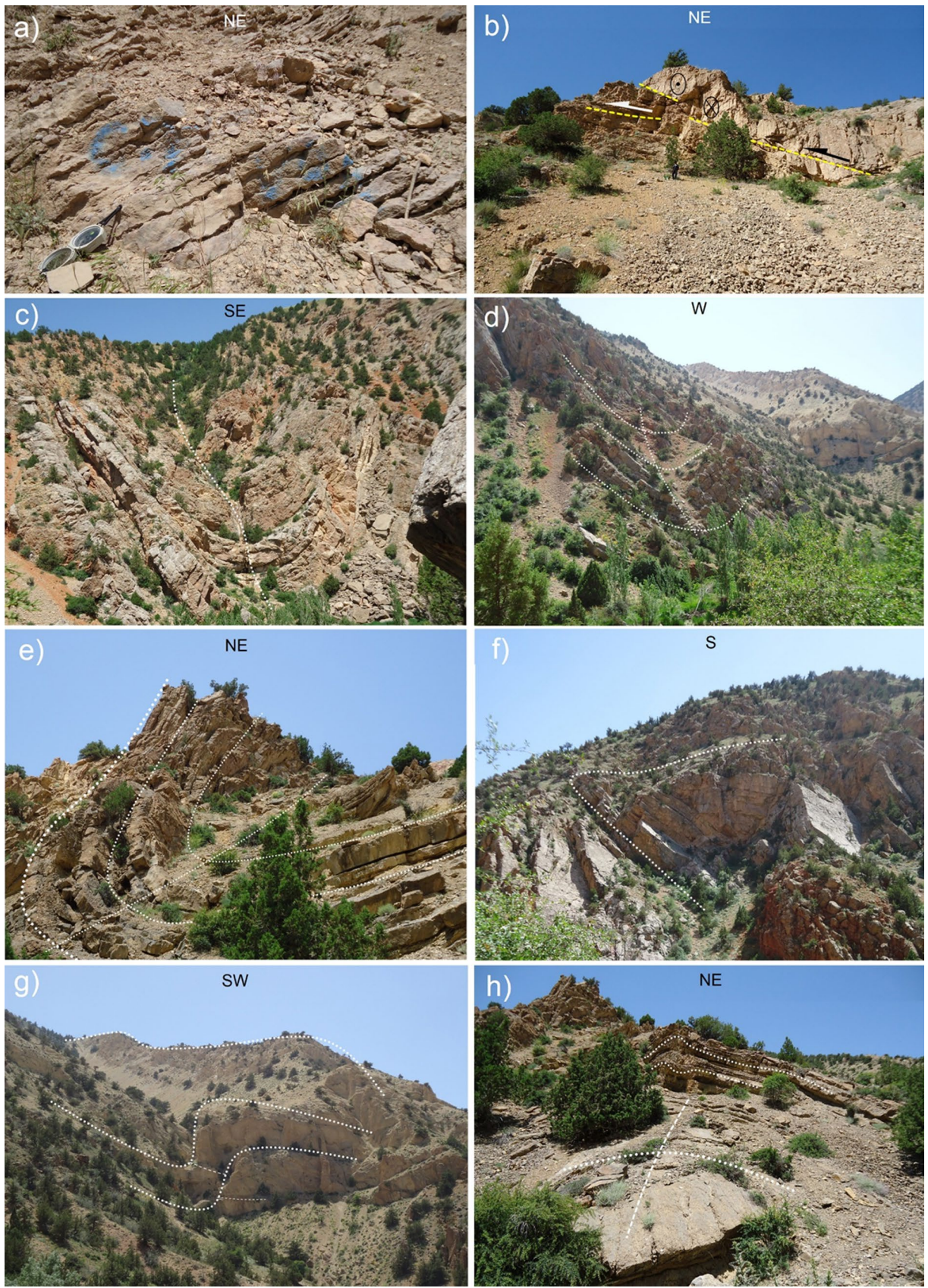
◀**Fig. 11** Some studied individual structural features in relation to transpression deformation zone. **a** Boudinage and pinch-and-swell structures in Ghalemoran and Ruteh Formations. **b** Multiple sets of faults (e.g. thrust and sinistral reverse faults seen in the Doroud Formation). **c–e** Plunging F2 folds in the Ruteh Formation (Fig. 11**c–e**), a highly curvilinear F2 buckle in the Ruteh Formation. **f** Recumbent F2 folds in the upper and younger sequences of the Ruteh Formation. **h** Asymmetric and overturned folds in Ghalemoran Formation (Fig. 11**g**), and also minor F2 folds in hinge of a major F2 fold in Ruteh Formation

axes (Nabavi 2012; Nabavi et al. 2014). These open folds can be classified as types C2, C3, D1, D2, E2 as in Hudleston's (1973) scheme (Nabavi 2012). Overturned and upright folds with a metric to decametric wavelengths and amplitudes formed in the Mobarak Formation and Ruteh and Doroud limestones (Nabavi 2012). These folds verge mainly between north-west and south-east (Table 3). The Santonian Ghalemoran Formation shows gentle folds and a break-thrust fold (Fischer et al. 1992; Woodward 1997) adjacent to the Chahar-bagh nappe. Break-thrust folds began as low-amplitude sinusoidal buckles with wavelengths controlled by the local stratigraphy. Break-thrust folds grow by folding with fixed hinges above and ahead of a propagating fault. Once the fold develops a tight interlimb angle (<10°) it locks and thrusts (Fischer et al. 1992; Woodward 1997). The axes of folds in both right and left stepping en-échelon arrays coincide with the regional NE–SW extensional axis that parallels the regional X axis major that is horizontal (e.g. Frehner 2016). These are too steep to have been shortened along the regional NW–SE compressional axis (Figs. 2c, 4a, 5f). En-échelon arrays of folds can form as a consequence of the regional simple shear strike–slip component and as drag folds in mesoscopic samples (Mukherjee et al. 2015).

Many ductile folds develop an axial plane foliation (Fig. 10b). This can indicate extension parallel to the orogeny and the formation of folds parallel to the maximum stretch (Watkinson 1975). Such orogen parallel extension is also highlighted by boudinage and pinch-and-swell structures of competent layers (in the Ghalemoran and Ruteh Formations) (Fig. 11a), with long axes sub-perpendicular to the stretching lineation.

Boudins in transpression zones indicate flattening (e.g. Zulauf et al. 2011a, b; Fossen et al. 2013). According to Jones et al.'s strain triangle (2004), many other structures in the study area are consistent with a transpressional regime. Examples are shown in Fig. 11a–h.

Multiple structures can also form in transpression during successive tectonic events with different kinematics. Indeed, all multiple structures could be attributed to separable deformation events or to a single, highly partitioned transpression or transtension event. To differentiate between these two options, we must consider the relative ages of each set of structures. We are pretty sure that they are all cotemporaneous, suggesting that they have been produced by a single transpressional event (e.g. Díaz-Azpiroz et al. 2014). Therefore, we attribute the periodic strain pattern across the study area ("Variation of strain parameters in space" section) to "ductile partitioning" in space (e.g. Schulmann et al. 2003). In this case, the regional transpression zone splits into pure shear zones in which strain accumulations decreased and wrench-dominated zones where strain accumulations increased.

Díaz-Azpiroz et al. (2014) proposed a new graph for inclined transpression. The main input parameters are as follows: (1) transpression obliquity (ϕ), defined as the angle between simple shear direction and the strike of the shear zone measured on vertical plane; (2) extrusion obliquity (υ), which is the angle between the extrusion direction of the coaxial component of the deformation and the dip direction of the shear zone; and (3) the kinematic vorticity number (W_k), a measure of the ratio between simple shear and pure shear. The angle of oblique convergence (α) is measured between the strike of the shear zone and the azimuth of the far-field vector (F_d), which defines the relative displacement of the undeformed blocks on both sides of the shear zone. The azimuth of the far-field vector coincides with the strike of the vorticity normal section (VNS), whose orientation can be estimated from ϕ and W_k (Jiang et al. 1998). According to Díaz-Azpiroz et al. (2014), the comparison between the natural data and the model is made following a standard procedure with three steps: (1) ϕ and υ values are constrained from geological observations; (2) the orientation of the finite strain ellipsoid is calculated; and (3) α value is calculated from the orientation of the shear zone.

In the regional deformation zone studied here, there is no evidence suggesting oblique extrusion. Therefore, the υ value has thus been taken as 0° (Fig. 12). According to our available data, the angle of oblique convergence is 31°–43° (average $\alpha = 37°$) (Fig. 12a). Inserting our angle of oblique convergence and dip of the shear zone into the following matrix (Jiang 2007, 2014) implies that the velocity gradient tensor of our transpressional zone is:

$$L = \begin{bmatrix} 0 & \cos(\alpha) & 0 \\ 0 & -\sin(\alpha)\cdot\sin(\delta) & 0 \\ 0 & \sin(\alpha)\cdot\cos(\delta) & \sin(\alpha)\cdot\sin(\delta) \end{bmatrix} = \begin{bmatrix} 0 & 0.765 & 0 \\ 0 & -0.414 & 0 \\ 0 & -0.492 & 0.414 \end{bmatrix}$$

(10)

Here the components of $-\sin(\alpha)\cdot\sin(\delta)$ and $\sin(\alpha)\cdot\sin(\delta)$ are the longitudinal strain rates parallel to the y axis and z axis, respectively. The components of $\cos(\alpha)$ and $\sin(\alpha)\cdot\cos(\delta)$ are the shear strain rates parallel to the x axis and z axis, respectively. This matrix can describe different
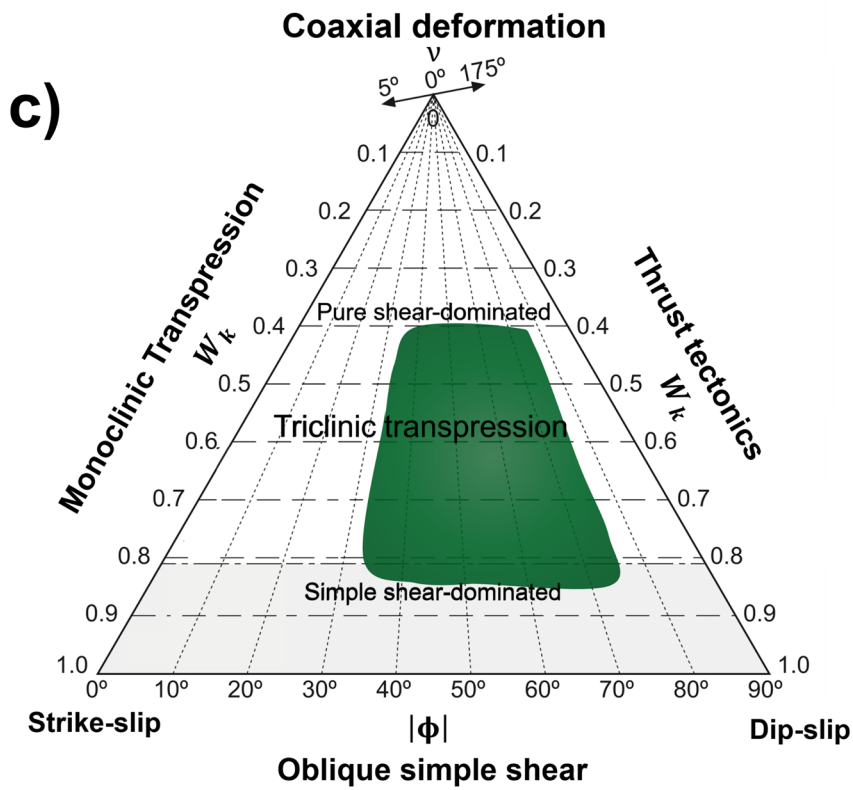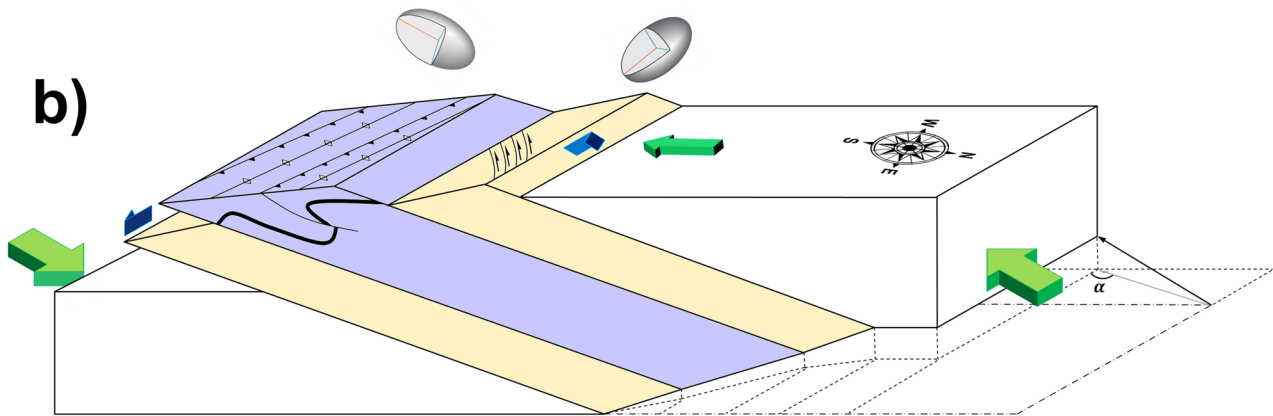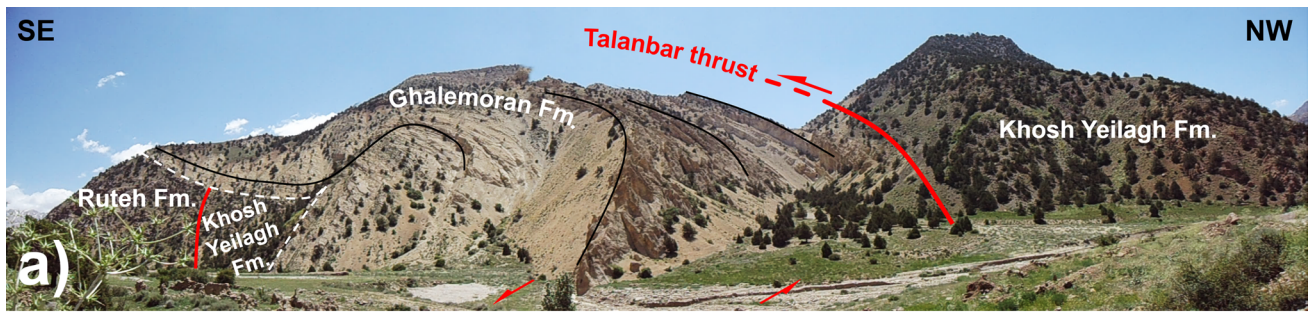
bulk flows, so that when $\alpha = 0°$ and $\delta = 90°$, the bulk flow is strike–slip simple shearing. When $0° < \alpha < 90°$ and $\delta = 90°$, the bulk flow is monoclinic transpression with a vertical shear boundary, and when $0° < \alpha < 90°$ and $0° < \delta < 90°$, the bulk flow is triclinic transpression with an inclined shear boundary.

In the following, we use an equal-area lower hemisphere plot with the orientation of the shear zone (with a strike N50°E and a dip of 37°NW), the angle of oblique convergence (α) (=31°–43°), and the dip of the zone (δ) (=37°) (Fig. 9b in Díaz-Azpiroz et al. 2014). In this plot, we can obtain the VNS great circle, the angle ϕ and angle Θ, which is defined as the angle between the horizontal velocity vector and the pole to the shear zone boundary. In 2D, W_k and the percentage of simple shearing and pure shearing may show a linear relationship, but not in 3D deformation. Hence, W_k can be expressed as a function of the simple shear-to-pure shear ratios, which equals the tangent of the angle Θ (Jiang et al. 1998). According to the simple shear-to-pure shear ratios estimated from W_k in Sect. 4.3, ϕ ranges between 36° and 75°, which indicates the study zone has triclinic symmetry (Fig. 8e).

Transpression zones in deformed domains can be partitioned (Fig. 12c) in the strain triangle of Jones et al. (2004). According to many studies on transpression, strain analysis and field observations, we can plot the study transpression onto the strain triangle. The vertices of the strain triangle show the special strain components which cover part of strain matrix, found in natural examples. The wrench corner illustrates the development of strike–slip faulting, Riedel shears or en-échelon folds on a map. The contractional corner illustrates the development of conjugate faults or symmetrical folds with hinges parallel to the strike. The dip-slip corner illustrates the development of dip-slip faults or asymmetric folds with hinges parallel to the regional strike. In this study, we use the new graphical method proposed by Díaz-Azpiroz et al. (2014) and use the orientation of the shear zone and its kinematic transpression parameters (Fig. 12c). This new graph is formed by incorporating Jones et al.'s (2004) strain triangle into the graph by Díaz-Azpiroz et al. (2014). According to the range of the kinematic vorticity number, field structures and the main

boundaries of the transpression zone studied, together with the strain matrices and nappe geometries, our main inclined transpression zone is a combination of all three components (as summarized in Fig. 12b). Our inclined (and/or oblique) transpression zone with its triclinic symmetry plots in the centre of the strain triangle (Fig. 12c). Triclinic transpression can be attributed to a horizontal velocity vector (V), which can be deduced from α and the strike of the zone boundaries to be N128°E.

Conclusions

We have interpreted brittle and ductile transpression structures in the outer eastern Alborz, particularly those structures in and near (<500 m) the inclined upper crustal transpression zone. The mechanical anisotropies in the sedimentary sequences deformed in the nappe increased structural heterogeneity throughout the progressive deformation. This led to a wide range of brittle and ductile structures with irregular and heterogeneous distributions across the nappe pile. In order to study the deformed rocks in the Neka Valley, we used field observations, analyses of fold geometries, and strain and the deformation matrices to study the partitioning.

The Ghalemoran and Doroud/Ruteh Formations in the Neka Valley are transpressed in a zone, bound by the Haji-abad and Shah-kuh thrusts, that strike 050°–060°, and dip 37° to the NW. The horizontal angle β (between the zone and its direction of overall shortening, S) is near 80°. These faults are linked westward to the North Alborz fault along strike by the sinistral strike–slip faults. En-échelon fold arrays with gently plunging axes trend NE–SW and step to both the right and left are attributed to strike–slip deformation components. Strain analysis of deformed macroscopic markers by the Fry (1979)'s method shows finite strain intensity values in oblate ellipsoids with $X{:}Y$ and $Y{:}Z$ ratios between 2.1 and 3.14. The average value of the regional vorticity number of $W_k = 0.6$ reveals contributions of 59 % pure shear and 41 % simple shear. These figures vary with distance from the basal thrusts within each nappe as cartooned in Fig. 9c. Strain analyses emphasize the heterogeneous nature of deformation in the Neka Valley. Variations in strain magnitudes and degree of non-coaxiality can be attributed to the geometry and orientation of the triaxial transpressional zone with respect to the transport direction along the NW to SE regional axis of shortening.

Strain partitioning and variations in strain intensity suggest strain heterogeneity on the map and its profiles. We attribute this partitioning to control by the angle of convergence between the Gondwana-derived Iran microplate with the southern margin of Eurasia in the Late Triassic, thereby closing the Paleo-Tethys. The obliquity of this convergence

ranges between 31° and 43° in the Neka Valley. Other notable factors controlling strain partitioning are differences in facies-type and lithologies (Mukherjee et al. 2012; Mukherjee 2015), and different rheologies (e.g. Mukherjee and Biswas 2015; Mulchrone and Mukherjee 2015). The ductility contrasts between the competent Devonian clastic-carbonate sequences of the Khosh Yeilagh Formation and relatively incompetent inoceramous, ooid and glauconitic bearing sandstones and limestones of the Santonian Ghalemoran Formation helped partition the orogen (e.g. Jones and Tanner 1995).

The shapes and orientations of local finite strain ellipsoid illustrate that any potentially ideal regional homogeneous deformation was affected by two factors: (1) the angle between the deformation zone boundaries and the shortening direction and (2) the exact path of the deformation. We attribute our transpression zone due to oblique convergence between two plates. Different shear senses can develop locally in the same deformation (Mukherjee 2013) as reported from the Zagros fold-and-thrust belt (Sarkarinejad et al. 2013). So too, the whole of the Alborz Mountains Range can be considered a curved inclined transpression zone with different shear senses on slightly different structural trends.

References

Abad I, Gutiérrez-Alonso G, Nieto F, Gertner I, Becher A, Cabero A (2003) The structure and the phyllosilicates (chemistry, crystallinity and texture) of Talas Ala-Tau (Tien Shan, Kyrgyz Republic): comparison with more recent subduction complexes. Tectonophysics 365:103–127

Alavi M (1996) Tectonostratigraphic synthesis and structural style of the Alborz Mountain system in northen Iran. J Geodyn 21:1–33

Allen MB, Ghassemi MR, Shahrabi M, Qorashi M (2003) Accommodation of late Cenozoic obliqe shortening in the Alborz range, northern Iran. J Struct Geol 25:659–672

Allen MB, Jackson J, Walker R (2004) Late Cenozoic reorganization of the Arabia-Eurasia collision and the comparison of short-term and long-term deformation rates. Tectonics 23:1–16

Angelier J (1989) From orientation to magnitudes in paleostress determinations using fault slip data. J Struct Geol 11:37–50

Angelier J, Mechler P (1977) Sur une methode graphique de recherché des contraintes principals également utilisable en tectonique et séismologie: la méthode des diedres droits. Bull Soc Géol Fr 19(6):1301–1318

Axen GJ, Lam PJ, Grove M, Stokli DF, Hassanzadeh J (2001) Exhumation of the west-central Alborz Mountains, Iran, Caspian subsidence, and collision-related tectonics. Geology 29:559–562

Axen GJ, Fakhari M, Guest B, Gavillot Y, Stokli DF, Horton B (2010) Distributed oblique-dextral transpression in the High Zagros Mountains, Iran. In: Tectonic Crossroads: evolving Orogens of Eurasia-Africa-Arabia, Ankara, Turkey, Abstracts, p 73

Babaahmadi A, Mohajjel M, Eftekhari A, Davodian AR (2012) An investigation into the fault patterns in the Chadegan region, west Iran: evidence for dextral brittle transpressional tectonics in the Sanandaj–Sirjan Zone. J Asian Earth Sci 43:77–88

Baikpour S, Talbot CJ (2012) The Garmsar salt nappe and seasonal inversions of surrounding faults imaged by SAR interferometry, Northern Iran. Geol Soc Lond Spec Publ 363(1):563–578

Balanyá JC, Crespo-Blanc A, Díaz-Azpiroz M, Expósito I, Juján M (2007) Structural trend line pattern and strain partitioning around the Gibraltar Arc accretionary wedge: insights as to the mode of orogenic arc building. Tectonics. doi:10.1029/2005TC001932

Ballato P, Uba CE, Landgraf A, Strecker MR, Sudo M, Stockli DF, Friedrich A, Tabatabaei SH (2011) Arabia-Eurasia continental collision: insights from the Tertiary foreland-basin evolution in the Alborz mountains, northern Iran. Geol Soc Am Bull 123:106–131

Ballato P, Stockli DF, Ghassemi MR, Landgraf A, Strecker MR, Hassanzadeh J, Friedrich A, Tabatabaei SH (2013) Accommodation of transpressional strain in the Arabia-Eurasia collision zone: new constraints from (U-Th)/He thermochronology in the Alborz mountains, north Iran. Tectonics. doi:10.1029/2012TC003159

Barcos L, Balanyá JC, Díaz-Azpiroz M, Expósito I, Jiménez-Bonilla A (2015) Kinematics of the Torcal Shear Zone: transpressional tectonics in a salient-recess transition at the northern Gibralter Arc. Tectonophysics (in press)

Bauer RL, Czeck DM, Hudleston PJ, Tikoff B (2011) Structural geology of the subprovince boundaries in the Archean Superior Province of northern Minnesota and adjacent Ontario. In: Miller JD, Hudak GJ, Witkop C, McLaughlin PI (eds) Archean to Anthropocene: Field Guides to the Geology of the Mid-Continent of North America, vol 24. Geological Society of America Field Guide, NewYork, pp 203–241

Berberian M, King GC (1981) Toward a paleogeography and tectonic evolution of Iran. Can J Earth Sci 18:210–265

Berra F, Zanchi A, Mattei M, Nawab A (2007) Late Cretaceous transgression on a Cimmerian high (Neka Valley, Eastern Alborz, Iran): a geodynamic event recorded by glauconitic sands. Sed Geol 199:189–204

Brun JP, Merle O (1985) Strain pattern in models of spreading-gliding nappes. Tectonics 4:705–719

Brun JP, Merle O (1988) Experiments on folding in spreading-gliding nappes. Tectonophysics 145:129–139

Capponi G, Carosi R, Meccheri M, Oggiano G (2003) Strain analysis in the Millen Range of Northern Victoria Land, Antarctica. Geologisches Jahrb B85:225–251

Carosi R, Palmeri R (2002) Orogen-parallel tectonic transport in the Variscan belt of northeastern Sardinia (Italy): implication for the exhumation of medium-pressure metamorphic rocks. Geol Mag 139:497–511

Carosi R, Di Pisa A, Lacopini D, Montomoli C, Oggiano G (2004) The structural evolution of the Asinara Island (NW Sardinia, Italy). Geodin Acta 175:309–329

Carosi R, Frassi C, Lacopini D, Montomoli C (2005) Post collisional transpressive tectonics in northern Sardinia (Italy). J Virtual Explor 19:1–30

Carreras J, Cosgrove JW, Druguet E (2013) Strain partitioning in banded and/or anisotropic rocks: implications for inferring tectonic regime. J Struct Geol 50:7–21

Cifelli F, Mattei M, Rashid H, Ghalamghash J (2013) Right-lateral transpressional tectonics along the boundary between Lut and Tabas blocks (Central Iran). Geophys J Int 193(3):1153–1165

Curtis ML (1993) The structural and kinematic evolution of an upper crustal transpression zone: the Lusitanian Basin, Portugal. Dissertation, University of Durham

Curtis ML (1997) Gondwanian age dextral transpression and spatial kinematic partitioning within the Heritage Range, Ellsworth Mountains, West Antarctica. Tectonics 16:172–181

Curtis ML (1998) Development of kinematic partitioning within a pure-shear dominated dextral transpression zone: the southern Ellsworth Mountains, Antarctica. In: Holdsworth RE, Strachan RA, Dewey JF (eds) Continental transpressional and transtensional tectonics. Geological Society of London, Special Publication 135, pp 289–306

Curtis ML, Flowerdew MJ, Riley TR, Whitehouse MJ, Daly JS (2010) Andean sinistral transpression and kinematic partitioning in South Georgia. J Struct Geol 32:464–477

Czeck D, Hudleston P (2003) Testing models for obliquely plunging lineations in transpression: a natural example and theoretical discussion. J Struct Geol 25:959–982

Czeck D, Hudleston P (2004) Physical experiments of vertical transpression with localized nonvertical extrusion. J Struct Geol 26:573–581

Dabo M, Aïfa T (2013) Pure shear to simple shear-dominated transpression during the Eburnean major D2 deformation, Daléma sedimentary basin, eastern Senegal. Int Geol Rev 55:1073–1086

Dabo M, Gueye M, Ngom PM, Diagne M (2008) Orogen-parallel tectonic transport: transpression and strain partitioning in the Mauritanides of NE Senegal. In: Ennih N, Liégeois J-P (eds) The boundaries of the West African Craton. Geological Society of London, Special Publication 297, pp 483–497

Dasgupta S, Mandal N, Bose S (2015) How far does a ductile shear zone permit transpression? In: Mukherjee S, Mulchrone KF (eds) Ductile shear zones: from micro- to macro-scales. Wiley, Chichester, pp 14–29

Davis JR, Titus SJ (2011) Homogeneous steady deformation: a review of computational techniques. J Struct Geol 33:1046–1062

Dehghani GA, Makris J (1984) The gravity field and crustal structure of Iran. Neues Jb Geol Paläontol Abh 168:215–229

Dewey J (1988) Extensional collapse of orogens. Tectonics 7(6):1123–1139

Dewey J (2002) Transtension in arc and orogens. Int Geol Rev 44:402–439

Dewey JF, Holdsworth RE, Strachan RA (1998) Transpression and transtension zones. In: Holdsworth RE, Strachan RA, Dewey JF (eds) Continental transpressional and transtensional tectonics. Geological Society, London, Special Publications 135, pp 1–14

Dias R, Ribeiro A (1994) Constriction in a transpressive regime: an example in the Iberian branch of the Ibero-Armorican arc. J Struct Geol 16:1543–1554

Díaz-Azpiroz M, Fernández C (2005) Kinematic analysis of the southern Iberian shear zone and tectonic evolution of the Acebuches metabasites (SW Variscan Iberian Massif). Tectonics. doi:10.1029/2004TC001682

Díaz-Azpiroz M, Barcos L, Balanyá JC, Fernández C, Expósito I, Czeck DM (2014) Applying a general triclinic transpression model to highly partitioned brittle–ductile shear zones: a case study from the Torcal de Antequera massif, external Betics, southern Spain. J Struct Geol 68:316–336

Dubey AK, Cobbold PR (1977) Noncylindrical flexural slip folds in nature and experiment. Tectonophysics 38:223–239

Dutton BJ (1997) Finite strain in transpression zones with no boundary slip. J Struct Geol 19:1189–1200

Faghih A, Kusky T, Samani B (2012) Kinematic analysis of deformed structures in a tectonic mélange: a key unit for the manifestation of transpression along the Zagros Suture Zone, Iran. Geol Mag 149:1107–1117

Fernández C, Díaz-Azpiroz M (2009) Triclinic transpression zones with inclined extrusion. J Struct Geol 31:1255–1269

Fernández C, Czeck DM, Díaz-Azpiroz M (2013) Testing the model of oblique transpression with oblique extrusion in two natural cases: steps and consequences. J Struct Geol 54:85–102

Fischer MP, Woodward NB, Mitchell MM (1992) The kinematic of break-thrust folds. J Struct Geol 14:451–460

Fleuty MJ (1964) The description of folds. Proc Geol Assoc 75(4):461–492

Fossen H (2016) Structural geology. Cambridge University Press, London

Fossen H, Tikoff B (1993) The deformation matrix for simultaneous simple shearing, pure shearing and volume change, and its application to transpression–transtension tectonics. J Struct Geol 15:413–422

Fossen H, Tikoff B (1998) Extended models of transpression and transtension, and application to tectonic settings. In: Holdsworth RE, Strachan RA, Dewey JF (eds) Continental transpressional and transtensional tectonics. Geological Society of London, Special Publication 135, pp 15–33

Fossen H, Tikoff B, Teyssier CT (1994) Strain modeling of transpressional and transtensional deformation. Nor Geol Tidsskr 74:134–145

Fossen H, Teyssier C, Whitney DL (2013) Transtensional folding. J Struct Geol 56:89–102

Frehner M (2016) 3D fold growth in transpression. Tectonophysics (in press)

Fry N (1979) Random point distribution and strain measurements. Tectonophysics 60:89–105

Ghosh SK (2001) Types of transpressional and transtensional deformation. In: Koyi HA, Mancktelow NS (eds) Tectonic modeling: a volume in honor of Hans Ramberg, vol 193. Geological Society of America Memoir, Boulder, CO, pp 1–20

Giorgis S, Tikoff B, McClelland W (2005) Missing Idaho arc: transpressional modification of the $^{87}Sr/^{86}Sr$ transition on the western edge of the Idaho batholith. Geology 33:469–472

González-Casado JM, Jiménez-Berrocoso Á, García-Cuevas C, Elorza J (2003) Strain determinations using inoceramid shells as strain markers: a comparison of the calcite strain gauge technique and the Fry method. J Struct Geol 25:1773–1778

Goodwin LB, Williams PF (1996) Deformation path partitioning within a transpressive shear zone, Marble Cove, Newfoundland. J Struct Geol 18:975–990

Guest B, Horton BK, Axen GJ, Hassanzadeh J, McIntosh WC (2007) Middle to late Cenozoic basin evolution in the western Alborz Mountains: implications for the onset of collisional deformation in northern Iran. Tectonics 26(6):TC6011. doi:10.1029/2006TC002091

Harland WB (1971) Tectonic transpression in Caledonian Spitsbergen. Geol Mag 108:27–42

Horsman E, Tikoff B, Czeck D (2008) Rheological implications of heterogeneous deformation at multiple scales in the Late Cretaceous Sierra Nevada, California. Geol Soc Am Bull 120:238–255

Horton BK, Hassanzadeh J, Stokli DF, Axen GJ, Gillis RJ, Guest B, Amini AH, Fakhri M, Zamanzadeh SM, Grove M (2008) Detrital zircon provenance of Neoproterozoic to Cenozoic deposits in Iran: implication for chronostratigraphy and collisional tectonics. Tectonophysics 451:97–122

Hossack J (1968) Pebble deformation and thrusting in the Bygdin area (Southern Norway). Tectonophysics 5:315–339

Hudleston PJ (1973) Fold morphology and some geometrical implications of theories of fold development. Tectonophysics 16:1–46

Hudleston PJ, Shultz-Ela D, Southwick D (1988) Transpression in an Archean greenstone belt, northern Minnesota. Can J Earth Sci 25:1060–1068

Iacopini D, Passchier CW, Koehn D, Carosi R (2007) Fabric attractors in general triclinic flow systems and their application to high strain shear zones; a dynamical system approach. J Struct Geol 29:298–317

Iacopini D, Carosi R, Montomoli C, Passchier CW (2008) Strain analysis and vorticity of flow in the northern Sardinian Variscan belt: recognition of a partitioned oblique deformation event. Tectonophysics 446:77–96

Jackson J, Priestley K, Allen M, Berberian M (2002) Active tectonics of the South Caspian Basin. Gephys J Int 148:214–245

Jiang D (2007) Sustainable transpression: an examination of strain and kinematics in deforming zones with migrating boundaries. J Struct Geol 29:1984–2005

Jiang D (2014) Structural geology meets micromechanics: a self-consistent model for the multiscale deformation and fabric development in Earth's ductile lithosphere. J Struct Geol 68:247–272

Jiang D, Lin S, Williams PF (1998) High-strain zones: a unified model. J Struct Geol 20:1105–1120

Jiang D, Lin S, Williams PF (2001) Deformation path in high-strain zones, with reference to slip partitioning in transpressional plate-boundary regions. J Struct Geol 23:991–1005

Jones RR, Holdsworth RE (1998) Oblique simple shear in transpression zones. In: Holdsworth RE, Strachan RA, Dewey JF (eds) Continental transpressional and transtensional tectonics. Geological Society, London, Special Publications 135, pp 35–40

Jones RR, Tanner PWG (1995) Strain partitioning in transpression zones. J Struct Geol 17:793–802

Jones RR, Holdsworth RE, Bailey W (1997) Lateral extrusion in transpression zones: the importance of boundary conditions. J Struct Geol 19:1201–1218

Jones RR, Holdsworth RE, Clegg P, McCaffrey KJW, Tavarnelli E (2004) Inclined transpression. J Struct Geol 26:1531–1548

Jones RR, Holdsworth RE, McCaffrey KJW, Clegg P, Tavarnelli E (2005) Scale dependence, strain compatibility and heterogeneity of three-dimensional deformation during mountain building: a discussion. J Struct Geol 27:1190–1204

Kassem OMK (2011) Determining heterogeneous deformation for granitic rocks in the northern thrust in Wadi Mubarak Belt, Eastern Desert, Egypt. Geotectonics 45:244–254

Kassem OMK (2014) Kinematic analysis of the Migif area in the Eastern Desert of Egypt. J Afr Earth Sc. doi:10.1016/j.jafrearsci.2014.02.002

Kassem OMK, Abd El Rahim SH (2010) Finite-strain analysis of Metavolcano-sedimentary rocks at Gabel El Mayet area, Central Eastern Desert, Egypt. J Afr Earth Sci 58:321–330

Kassem OMK, Ring U (2004) Underplating-related finite-strain patterns in the Gran Paradiso massif, Western Alps, Italy: heterogeneous ductile strain superimposed on a nappe stack. J Geol Soc Lond 161:875–884

Kassem OMK, Abd El Rahim SH, El Nashar ESR (2012) Strain analysis and microstructural evolution characteristic of neoproterozoic rocks associations of Wadi El Falek, centre Eastern Desert, Egypt. Geotectonics 46:379–388

Kuiper YD, Lin S, Jiang D (2011) Deformation partitioning in transpressional shear zones with an along-strike stretch component: an example from the Superior Boundary Zone, Manitoba, Canada. J Struct Geol 33:192–202

Landgraf A, Ballato P, Strecker MR, Friedrich A, Tabatabaei SH, Shahpasandzadeh M (2009) Fault-kinematic and geomorphic observations along the North Tehran Thrust and Mosha Fasham Fault, Alborz mountains, Iran: implicatios for fault-system evolution and interaction in a changing tectonic regime. Geophys J Int 177(2):676–690

Law RD, Searle MP, Simpson RL (2004) Strain, deformation tempratures and vorticity of flow at the top of the Greater Himalayan Slab, Everest Massif, Tibet. J Geol Soc Lond 161:305–320

Lin S, Jiang D, Williams PF (1998) Transpression (or transtension) zones of triclinic symmetry: natural example and theoretical modelling. In: Holdsworth RE, Strachan RA, Dewey JF (eds) Continental transpressional and transtensional tectonics. Geological Society, London, Special Publications 135, pp. 41–57

Lister GS, Williams PF (1983) The partitioning of deformation in flowing rock masses. Tectonophysics 92:1–33

Liu X, McNally KC, Shen ZK (1995) Evidence for a role of the down going slab in earthquake partitioning at oblique subduction zones. J Geophys Res 100:15351–15372

Massey MA, Moecher DP (2013) Transpression, extrusion, partitioning, and lateral escape in the middle crust: significance of structures, fabrics, and kinematics in the Bronson Hill zone, southern New Zealand, USA. J Struct Geol 55:62–78

McCaffrey R (1992) Oblique plate convergence, slip vectors, and forearc deformation. J Geophys Res 97:8905–8915

McClusky S, Reilinger R, Mahmoud S, Ben Sari D, Tealeb A (2003) GPS constraints on Africa (Nubia) and Arabia plate motions. Geophys J Int 155(1):126–138

Means WD, Hobbs BE, Lister BE, Williams PF (1980) Vorticity and non-coaxility in progressive deformations. J Struct Geol 2:371–378

Merle O (1986) Patterns of stretch trajectories and strain rate within spreading-gliding nappes. Tectonophysics 124:211–222

Milnes AG (1994) Aspects of 'strike-slip' or wrench tectonics—an introductory discussion. Nor Geol Tidsskr 74:129–133

Mohajjel M, Fergusson CL (2000) Dextral transpression in Late Cretaceous continental collision, Sanandaj–Sirjan zone, western Iran. J Struct Geol 22:1125–1139

Mohajjel M, Fergusson CL, Sahandi MR (2003) Cretaceous–Tertiary convergence and continental collision, Sanandaj–Sirjan zone, eastern Iran. J Asian Earth Sci 21:397–412

Moosavi E, Mohajjel M, Rashidnejad-Omran N (2014) Systematic changes in orientation of linear mylonitic fabrics: an example of strain partitioning during transpressinal deformation in north Golpaygan, Sanandaj–Sirjan zone, Iran. J Asian Earth Sci 94:55–67

Mukherjee S (2007) Geodynamics, deformation and mathematical analysis of metamorphic belts of the NW Himalaya. Unpublished Ph.D. thesis. Indian Institute of Technology, Roorkee, pp 1-267

Mukherjee S (2011a) Mineral fish: their morphological classification, usefulness as shear sense indicators and genesis. Int J Earth Sci 100:1303–1314

Mukherjee S (2011b) Flanking microstructures from the Zanskar Shear zone, NW Indian Himalaya. YES Netw Bull 1:21–29

Mukherjee S (2012a) Simple shear is not so simple! Kinematics and shear senses in Newtonian viscous simple shear zones. Geol Mag 149:819–826

Mukherjee S (2012b) Tectonic implications and morphology of trapezoidal mica grains from the Sutlej section of the Higher Himalayan Shear Zone, Indian Himalaya. J Geol 120:575–590

Mukherjee S (2013) Deformation microstructures in rocks. Springer, NewYork

Mukherjee S (2014a) Review of flanking structures in meso- and micro-scales. Geol Mag 151:957–974

Mukherjee S (2014b) Mica inclusions inside host mica grains from the Sutlej Section of the Higher Himalayan Crystallines, India—Morphology and Constrains in Genesis. Acta Geol Sinica 88:1729–9741

Mukherjee S (2014c) Kinematic of 'top-to-down' simple shear in a Newtonian rheology. J Indian Geophys Union 18:245–248

Mukherjee S (2014d) Atlas of shear zone structures in meso-scale. Springer, Berlin

Mukherjee S (2015) A review on out-of-sequence deformation in the Himalaya. In: Mukherjee S, Carosi R, van der Beek P, Mukherjee BK, Robinson D (Eds) Tectonics of the Himalaya. Geological Society of London, Special Publication 312, 67–109

Mukherjee S, Biswas R (2014) Kinematics of horizontal simple shear zones of concentric arcs (Taylor Couette flow) with incompressible Newtonian rheology. Int J Earth Sci 103:597–602

Mukherjee S, Biswas R (2015) Biviscous horizontal simple shear zones of concentric arcs (Taylor Couette flow) with incompressible Newtonian rheology. In: Mukherjee S, Mulchrone KF (eds) Ductile Shear Zones: from micro- to macro-scales. Wiley, Chichester, pp 59–62

Mukherjee S, Koyi HA (2009) Flanking microstructures. Geol Mag 146(04):517

Mukherjee S, Koyi HA (2010) Higher Himalayan Shear Zone, Sutlej section: structural geology and extrusion mechanism by various combinations of simple shear, pure shear and channel flow in shifting modes. Int J Earth Sci 99:1267–1303

Mukherjee S, Mulchrone KF (2012) Estimating the viscosity and Prandtl number of the Tso Morari crystalline gneiss dome, Indian western Himalaya. Int J Earth Sci 101(7):1929–1947

Mukherjee S, Koyi HA, Talbot C (2012) Implications of channel flow analogue models in extrusion of the Higher Himalayan Shear Zone with special reference to the out-of-sequence thrusting. Int J Earth Sci 101:253–272

Mukherjee S, Punekar J, Mahadani T, Mukherjee R (2015) A review on intrafolial folds and their morphologies from the detachments of the western Indian Higher Himalaya. In: Mukherjee S, Mulchrone KF (eds) Ductile Shear Zones: from micro- to macro-scales. Wiley, Chichester, pp 182–205

Mulchrone KF (2013) Qualitative and quantitative analysis of vorticity, strain and area change in general non-isochroic 2D deformation. J Struct Geol 55:114–126

Mulchrone KF, Mukherjee S (2015) Shear senses and viscous dissipation of layered ductile simple shear zones. Pure Appl Geophys 172:2635–2642

Nabavi ST (2012) Emplacement mechanism of fold-and-thrust nappes in Chahar-bagh area, Eastern Alborz. Dissertation, Damghan University

Nabavi ST, Khademi M, Rahimi-Chakdel A (2014) Inclined transpression deformation zone of Chahr-bagh nappe, eastern Alborz. J Tecton Struct 2:56–76 **(In Persian with English abstract)**

Nabavi ST, Samani B, Khademi M, Rahimi-Chakdel (in preparation) Implications of strain and vorticity analyses to interpret the rear compression emplacement mechanism in the Chahar-bagh nappe, Eastern Alborz, Iran

Naylor MA, Mandl G, Sijpesteijn CHK (1986) Fault geometries in basement-induced wrench faulting under different initial stress states. J Struct Geol 8:737–752

O'Hara KD (1990) State of strain in mylonites from the western Blue Ridge province, south Appalachians: the role of volume loss. J Struct Geol 12:419–430

Oldow JS, Bally AW, Avé Lallemant HG (1990) Transpression, orogenic float, and lithospheric balance. Geology 8:991–994

Passchier CW (1987) Stable positions of rigid objects in non-coaxial flow: a study in vorticity analysis. J Struct Geol 9:679–690

Passchier CW (1998) Monoclinic model shear zones. J Struct Geol 20:1121–1137

Passchier CW, Trouw RAJ (2005) Microtectonics. Springer, Berlin

Pollard DD, Fletcher RC (2005) Fundamental of structural geology. Cambridge University Press, Cambridge

Provost A, Buisson C, Merle O (2004) From progressive to finite deformation and back. J Geophys Res. doi:10.1029/2001JB001734

Ramberg H (1975) Superposition of homogeneous strain and progressive deformation in rocks. Bull Geol Inst 6:35–67

Ramsay JG (1967) Folding and fracturing of rocks. McGraw-Hill, New York

Ramsay JG, Graham RM (1970) Strain variation in shear belts. Can J Earth Sci 7:786–813

Ramsay JG, Huber MI (1983) The techniques of modern structural geology: strain analysis, vol 1. Academic Press, London

Ritz J-F (2009) Extrusion tectonics and subduction in the eastern South Caspian region since 10 Ma: comment. Geology 37:e191

Ritz J-F, Nazari H, Ghassemi A, Salamati R, Shafei A, Solaymani S, Vernant P (2006) Active transtension inside central Alborz: a new insight into northern Iran-southern Caspian geodynamics. Geology 34:477–480

Robin P-YF, Cruden AR (1994) Strain and vorticity patterns in ideally ductile transpression zones. J Struct Geol 16:447–466

Roday P, Purohit MK, Prajapati KK (2010) A compute program for the determination of finite strain using Fry method. J Geol Soc India 76:151–154

Rodriguez J, Coke C, Dias R, Pereira E, Ribeiro A (2005) Transition from autochthonous to parautochthonous deformation regimes in Murca-Marão sector (Central-Iberian Zone, northern Portugal). J Virtual Explor. doi:10.3809/jvirtex.2005.00124

Sanderson DJ (2014) Transpression/transtension: a model for micro- to macro-scale deformation. In: EGU General assembly conference abstracts, vol 16, p 16943

Sanderson DJ, Marchini WRD (1984) Transpression. J Struct Geol 6:449–458

Sarkarinejad K (2007) Quantitative finite strain and kinematic flow analyses along the Zagros transpression zone, Iran. Tectonophysics 442:49–65

Sarkarinejad K, Azizi A (2008) Slip partitioning and inclined dextral transpression along the Zagros Thrust system, Iran. J Struct Geol 30:116–136

Sarkarinejad K, Faghih A, Grasemann B (2008) Transpressional deformation within the Sanandaj–Sirjan metamorphic belt (Zagros Mountains, Iran). J Struct Geol 30:818–826

Sarkarinejad K, Heyhat M, Faghih A, Kusky T (2010a) Heterogeneous ductile deformation and quartz c-axis fabric development within the HP-LT Sanandaj–Sirjan Metamorphic Belt, Iran. Tectonophysics 485:283–289

Sarkarinejad K, Samani B, Faghih A, Grasemann B, Moradipoor M (2010b) Implication of strain and vorticity of flow analyses to interpret the kinematics of an oblique convergence event (Zagros Mountains, Iran). J Asian Earth Sci 38:34–43

Sarkarinejad K, Partabian A, Faghih A, Kusky TM (2012) Usage of strain and vorticity analyses to interpret large-scale fold mechanisms along the Sanandaj-Sirjan metamorphic belt, SW Iran. Geol J 47(1):99–110

Sarkarinejad K, Partabian A, Faghih A (2013) Variation in the kinematics of deformation along the Zagros inclined transpression zone, Iran: implications for defining a curved inclined transpression zone. J Struct Geol 48:126–136

Schulmann K, Thompson AB, Lexa O, Ježek J (2003) Strain distribution and fabric development modelled in active and ancient transpressive zones. J Gephys Res. doi:10.1029/2001JB000632

Shafiei Bafti S, Mohajjel M (2015) Structural evidence for slip partitioning and inclined dextral transpression along the SE Sanandaj–Sirjan zone, Iran. Int J Earth Sci 104:587–601

Shahrabi M (1990) Geological Survey of Iran, Quadrangle map of Gorgan, scale 1:250000

Simpson C, De Paor DG (1993) Strain and kinematic analysis in general shear zones. J Struct Geol 15:1–20

Sullivan WA, Law RD (2007) Deformation path partitioning within the transpressional White Mountain shear zone, California and Nevada. J Struct Geol 29:583–598

Sylvester AG (1988) Strike-slip faults. Geol Soc Am Bull 100:1666–1703

Talbot CJ (2014) Lessons from the first 100 minimum strain ellipsoids constrained in gneisses deformed at high metamorphic grade. Earth Sci Rev 138:231–267

Talbot CJ, Aftabi P (2004) Geology and models of salt extrusion at Qum Kuh, central Iran. J Geol Soc Lond 161:321–334

Talbot CJ, Pohjola V (2009) Subaerial salt extrusion in Iran as analogues of ice sheets, streams and glaciers. Earth Sci Rev 97:167–195

Talbot CJ, Sokoutis D (1995) Strain ellipsoids from incompetent dykes: application to volume loss during mylonitization in the Singo gneiss zone, central Sweden. J Struct Geol 17:927–948

Tavarnelli E, Holdsworth RE (1999) How long do structure take to form in transpression zones? A cautionary tale from California. Geology 27:1063–1066

Tavarnelli E, Holdsworth RE, Clegg P, Jones RR, McCaffrey KJW (2004) The anatomy and evolution of a transpressional imbricate zone, South Uplands, Scotland. J Struct Geol 26:1341–1360

Teyssier C, Tikoff B (1999) Fabric stability in oblique convergence and divergence. J Struct Geol 21:969–974

Teyssier C, Tikoff B, Markley M (1995) Oblique plate motion and continental tectonics. Geology 23:447–450

Tikoff B, Fossen H (1993) Simultaneous pure and simple shear: the unifying deformation matrix. Tectonophysics 217:267–283

Tikoff B, Fossen H (1995) The limitation of three-dimensional kinematic vorticity analysis. J Struct Geol 17:1771–1784

Tikoff B, Fossen H (1999) Three-dimensional reference deformations and strain facies. J Struct Geol 21:1497–1512

Tikoff B, Greene D (1997) Stretching lineations in transpressional shear zones: an example from the Sierra Nevada Batholith, California. J Struct Geol 19:29–39

Tikoff B, Paterson K (1998) Physical experiments of transpressional folding. J Struct Geol 20:661–672

Tikoff B, Teyssier C (1994) Strain modelling of displacement-field partitioning in transpressional orogens. J Struct Geol 16:1557–1588

Titus SJ, Housen B, Tikoff B (2007) A kinematic model for the Rinconada fault system in central California based on structural analysis of en echelon folds and paleomagnetism. J Struct Geol 29:961–982

Treagus JE, Treagus SH (1981) Folds and the strain ellipsoid: a general model. J Struct Geol 3:1–17

Tripathy NR, Srivastava HB, Mamtani MA (2009) Evaluation of a regional strain gradient in mylonitic quartzites from the footwall of the Main Central Thrust Zone (Garhwal Himalaya, India): inferences from finite strain and AMS analyses. J Asian Earth Sci 34:26–37

Twiss RJ, Moores EM (2007) Structural geology, 2nd edn. Freeman and Company, New York

Vernant P, Nilforoushan F, Hatzfeld D, Abbassi M, Vigny C, Masson F, Nankali H, Martinod J, Ashtari A, Bayer R, Tavakoli F, Chry J (2004) Present-day crustal deformation and plate kinematics in the Middle East constrained by GPS measurements in Iran and northern Oman. Geophys J Int 157:381–398

Viola G, Henderson IC (2010) Inclined transpression at the toe of an arcute thrust: an example from the Precambrian 'Mylonite Zone' of the Sveconorwegian orogeny. Geol Soc Lond Spec Publ 335:715–737

Wallis SR (1992) Vorticity analysis in a metachert from the Sanbagawa belt, SW Japan. J Struct Geol 14:271–280

Wallis SR (1995) Vorticity analysis and recognition of ductile extension in the Sanbagawa belt, SW Japan. J Struct Geol 17:1077–1093

Watkinson A (1975) Multilayer folds initiated in bulk plane strain with the axis of no change perpendicular to the layering. Tectonophysics 28:T7–T11

Woodcock NH, Schubert C (1994) Continental strike-slip tectonics. In: Hancock PL (ed) Continental tectonics. Pergamon, Oxford, pp 251–263

Woodward NB (1997) Low-amplitude evolution of break-thrust folding. J Struct Geol 19:293–301

Xypolias P (2010) Vorticity analysis in shear zones: a review of methods and applications. J Struct Geol 32:2072–2092

Zanchi A, Berra F, Mattei M, Ghassemi MR, Sabouri J (2006) Inversion tectonics in Central Alborz, Iran. J Struct Geol 28:2023–2037

Zanchi A, Zanchetta S, Berra F, Mattei M, Garzanti E, Molyneux S, Nawab A, Sabouri J (2009) The Eo-Cimmerian orogeny in North Iran. In: Brunet M-F, Wilmsen M, Granath JW (eds) South Caspian to Central Iran Basins. Geological Society of London, Special Publications 312, pp 31–55

Zibra I, Smithies RH, Wingate MTD, Kirkland CL (2014) Incremental pluton emplacement during inclined transpression. Tectonophysics 623:100–122

Zulauf J, Gutiérrez-Alonso G, Kraus R, Petschick R, Potel S (2011a) Formation of chocolate-tablet boudins in a foreland fold and thrust belt: a case study from the external Variscides (Almograve, Portugal). J Struct Geol 33:1649–1939

Zulauf J, Zulauf G, Kraus R, Gutiérrez-Alonso G, Zanella F (2011b) The origin of tablet boudinage: results from experiments using power-law rock analogs. Tectonophysics 510:327–336